Monthly Notices
of the
ROYAL ASTRONOMICAL SOCIETY

MNRAS **459,** 2212–2236 (2016)
Advance Access publication 2016 April 6

doi:10.1093/mnras/stw782

Galaxy evolution in nearby galaxy groups – III. A *GALEX* view of NGC 5846, the largest group in the local universe

Antonietta Marino,[1★] Paola Mazzei,[1] Roberto Rampazzo[1] and Luciana Bianchi[2]

[1]*INAF – Osservatorio Astronomico di Padova, vicolo dell'Osservatorio 5, I-35122 Padova, Italy*
[2]*Department of Physics and Astronomy, Johns Hopkins University, 3400 North Charles Street, Baltimore, MD 21218, USA*

Accepted 2016 April 1. Received 2016 February 18; in original form 2015 October 19

ABSTRACT

We explore the co-evolution of galaxies in nearby groups ($V_{\rm hel} \leq 3000$ km s^{-1}) with a multiwavelength approach. We analyse *GALEX* far-UV (FUV) and near-UV (NUV) imaging, and Sloan Digital Sky Survey *u*, *g*, *r*, *i*, *z* data of groups spanning a large range of dynamical phases. We characterize the photometric properties of spectroscopically confirmed galaxy members and investigate the global properties of the groups through a dynamical analysis. Here, we focus on NGC 5846, the third most massive association of early-type galaxies (ETGs) after the Virgo and Fornax clusters. The group, composed of 90 members, is dominated by ETGs (about 80 per cent), and among ETGs about 40 per cent are dwarfs. Results are compared with those obtained for three groups in the LeoII cloud, which are radically different both in member-galaxy population and dynamical properties. The FUV–NUV cumulative colour distribution and the normalized UV luminosity function (LF) significantly differ due to the different fraction of late-type galaxy population. The UV LF of NGC 5846 resembles that of the Virgo cluster, however our analysis suggests that star formation episodes are still occurring in most of the group galaxies, including ETGs. The NUV$-i$ colour distribution, the optical–UV colour–colour diagram, and NUV$-r$ versus M_r colour–magnitude relation suggest that the gas contribution cannot be neglected in the evolution of ETG-type group members. Our analysis highlights that NGC 5846 is still in an active phase of its evolution, notwithstanding the dominance of dwarf and bright ETGs and its virialized configuration.

Key words: galaxies: evolution – galaxies: formation – galaxies: groups: individual: NGC 5846 group, USGC U677 – galaxies: kinematics and dynamics – galaxies: photometry – Ultraviolet: galaxies.

1 INTRODUCTION

The study of the co-evolution of galaxies in groups is crucial to address the problem of the star formation quenching and galaxy morphological transformations, as groups contain most (∼60 per cent) of the galaxies in the Universe at the present day (e.g. Tully 1988; Ramella et al. 2002; Eke et al. 2004; Tago et al. 2008), and most of the stellar mass is formed in groups. The transition between galaxy properties typical of field and clusters happens just at the characteristic densities of groups, suggesting the existence of evolutionary mechanisms acting before galaxies in groups fall into clusters (Lewis et al. 2002; Gómez et al. 2003). Such re-processing mechanisms act by transforming field, i.e. spiral galaxies, to cluster-like galaxies, i.e. early-type galaxies (ETGs), and basically drive groups from an 'active' (star-forming) phase, typical of field, to a more 'passive' phase, typical of clusters (e.g. Gómez et al. 2003; Goto et al. 2003). Evidence in this sense comes from a number of 'classical' studies on the impact of environment on galaxy properties showing that ETGs are more strongly clustered than late-type galaxies (e.g Davis & Geller 1976). Dressler (1980) showed that the fraction of elliptical and S0 galaxies is higher in denser environments. By now, it is widely accepted that galaxies in clusters tend to have depressed star formation rates in comparison with the field population (e.g. Balogh et al. 2004; Poggianti et al. 2006, and references therein).

Several physical processes are believed to play a role in galaxy evolution and star formation variations. They have been inferred both from observations and simulations and there is a wide consensus that they are different in rich and poor galaxy environments. Mergers can transform spirals into ellipticals (Toomre & Toomre 1972; Barnes 2002), and quench star formation by ejecting the interstellar medium via starburst, active galactic nucleus or shock-driven winds (e.g. Di Matteo, Springel & Hernquist 2005). Since velocity dispersions of groups are comparable to the velocity dispersion of individual galaxies, both interactions and merging are

★ E-mail: antonietta.marino@oapd.inaf.it

more favoured in groups than in clusters (Mamon 1992) as well as phenomena like 'galaxy strangulation' (Kawata & Mulchaey 2008). Transforming mechanisms in rich environments should act through galaxy–galaxy 'harassment' and ram-pressure (see e.g. Moore et al. 1996).

The dramatic evidence of galaxy transformation has been obtained with *GALEX*. UV–optical colour–magnitude diagrams (CMD) evidenced not only a sequence of red galaxies, mostly ETGs, and a 'blue cloud' mainly composed of late-type galaxies, but also an intermediate region, the 'green valley', populated of transforming galaxies (Schawinski et al. 2007).

We are exploring the co-evolution of galaxies in groups in the local Universe by adopting a multiwavelength approach. We use UV and optical imaging to analyse a set of nearby groups spanning a large range of evolutionary phases. In particular, *GALEX* UV wide-field imaging, made it possible to directly map present-day star formation, ranking groups according to their blue and red galaxy population. Moreover, we analyse group compactness, a signature of the evolutionary phase, through a kinematic and dynamical analysis. To further investigate the transition from active groups to more evolved passive systems, we select groups with different properties, from late-type galaxy dominated groups, analogues of our Local Group (Marino et al. 2010, hereafter Paper I), to groups with an increasing fraction of ETGs, increasing signatures of interaction, and advanced stage of virialization (Marino et al. 2013, hereafter Paper II).

In order to investigate the transition between active groups and more evolved passive systems, we analyse in this paper the NGC 5846 group, that in the Ramella et al. (2002) catalogue is labelled as USGC U677.

Ferguson & Sandage (1991) showed that the dwarf-to-giant ratio increases with the richness of the group. Eigenthaler & Zeilinger (2010) estimated the early-type-dwarf-to-giant-ratio (EDGR) (i.e. dE+dE,N+dS0 to E+S0) for NGC 5486 group obtaining EDGR = 2.69. In the Local Supercluster, this value is exceeded only by Virgo (EDGR = 5.77) and Fornax (EDGR = 3.83) clusters indicating that NGC 5846 is the third more massive galaxy aggregate. The group is dominated by two bright ETGs, NGC 5846 and NGC 5813, that do not show clear signatures of interaction in UV and optical images. X-ray studies revealed the presence of an extended (50–100 kpc radius) halo of NGC 5846, and numerous peculiar features, cavities and bubbles in both galaxies (Trinchieri & Goudfrooij 2002; Mulchaey et al. 2003; Werner et al. 2009, 2014; Machacek et al. 2011; Randall et al. 2011). These two X-ray haloes suggested the presence of substructures in the NGC 5846 group and motivated a wide literature about the determination of group members (e.g. Tully 1987; Haynes & Giovanelli 1991; Nolthenius 1993; Giuricin et al. 2000; Ramella et al. 2002; Mahdavi, Trentham & Tully 2005; Eigenthaler & Zeilinger 2010). The low optical luminosity galaxy population has been studied by Mahdavi et al. (2005) and Eigenthaler & Zeilinger (2010): nucleated dwarfs reside near the bright members, and only four dwarfs show fine structures or interaction signatures. At odd, signatures of activity are found in the inner part of the two bright members. Werner et al. (2014) detected H α+[N II] at kpc scale and [C II] $\lambda = 157$ µm emission in both galaxies. Rampazzo et al. (2013), using *Spitzer*, detected mid-infrared lines like [Ne II] $\lambda = 12.81$ µm, [Ne III]$\lambda = 15.55$ µm and some H_2 (0–0) lines in both galaxies.

Although NGC 5846 is the third most massive association of ETGs after Virgo and Fornax, its UV properties are still unknown and this motivates the present study. The paper is arranged as follows. Section 2 discusses the criteria adopted to select the galaxy members, and the group kinematical and dynamical properties. Section 3 presents the UV and optical observations and data reduction. The photometric results are given in Section 4. Section 5 and 6 focus on the discussion and our conclusions, respectively. $H_0 =$ 75 km s^{-1} Mpc^{-1} is used throughout the paper but for luminosity function, where in agreement with Boselli & Gavazzi (2014) a value of 70 km s^{-1} Mpc^{-1} is adopted.

2 MEMBERSHIP AND DYNAMICAL ANALYSIS OF THE GROUP

2.1 Selection of the NGC 5846 group members

We follow the approach developed in our Paper I and II. Briefly, once characterized the group through a density analysis of a region of 1.5 Mpc of diameter around the B brightest member, we revise the group membership using recent redshift surveys. For each member galaxy, we investigate morphology and measure surface photometry in FUV, NUV, and optical *u*, *g*, *r*, *i*, *z* bands.

As described in more detail in Paper II, the group sample has been selected starting from the catalogue of Ramella et al. (2002) which lists 1168 groups of galaxies covering 4.69 steradians to a limiting magnitude of $m_B \approx 15.5$. The member galaxies of the catalogue were cross-matched with the *GALEX* and Sloan Digital Sky Survey (SDSS) archives in order to select groups covered by both surveys. We chose only groups within 40 Mpc, i.e. with a heliocentric radial velocity $V_{\rm hel} < 3000$ km s^{-1}, and composed of at least eight galaxies to single out intermediate and rich structures. The above criteria led to a sample of 13 nearby groups having between 8 and 47 members listed in the catalogue of Ramella et al. (2002). Their fraction of ETGs, according to the Hyper-Lyon-Meudon Extragalactic Database (Makarov et al. 2014, HYPERLEDA hereafter), ranges from the same fraction as in the field, i.e. ≈15–20 per cent, to a value typical of dense environments, ≈80–85 per cent (e.g. Dressler 1980). UV and optical data are available for most of their galaxy members and we further obtained new NUV imaging of most of the remaining galaxies in the *GALEX* GI6 programmme 017 (PI A. Marino).

We focus here on NGC 5846 group. In the catalogue of Ramella et al. (2002), the group, named USGC U677, is composed of 17 members with $\langle V_{\rm hel}\rangle \sim 1634 \pm 117$ km s^{-1} and has an average apparent B magnitude of $\langle B_T\rangle \sim 11.64 \pm 2.07$ mag. According to the HYPERLEDA classification, the group is dominated by ETGs, whose percentage achieves ~70 per cent, similar to that in clusters. We further include as group members all the galaxies in the HYPERLEDA catalogue with a heliocentric radial velocity within $\pm 3\sigma$ the group average velocity, $\langle V_{hel}\rangle$, and within a diameter of ~1.5 Mpc around the centre of the group given by Ramella et al. (2002).

Table 1 lists the properties of the 90 galaxies selected using the method described above. Columns from 1 to 12 provide our ID member number, the galaxy name, J2000 coordinates, morphological type, heliocentric velocity, B total apparent magnitude, major axis diameter, D_{25}, axial ratio, position angle, inclination and the foreground galactic extinction, respectively. The morphological type is taken from HYPERLEDA. This catalogue associates a type, T, to the morphological classification. Galaxies with T ≤ 0 are considered early-type. Ellipticals are in the range $-5 \leq T \leq -3$, Spirals have T ≥ 0. Dwarf galaxies are not fully considered in this classification. However, Sm, magellanic Irr, (T = 9) and generic Irr (T = 10) are dwarfs. Dwarf early-type are not classified in the HYPERLEDA scheme. We adopt for them the same classification

Table 1. Journal of the galaxy members[a].

Id. No.	Galaxy	RA (J2000) (deg)	Dec. (J2000) (deg)	Morph. type (^{a} — ^{b})	Mean Hel. Vel (km s^{-1})	B_T (mag)	D_{25} (arcsec)	log r_{25}	PA (deg)	Incl. (deg)	$E(B-V)$ (mag)
1	PGC053384	224.005 05	2.463 58	S0-a — ...	2109 ± 22	15.20 ± 0.44	58.6	0.45	171.3	90	0.038
2	PGC1186917	224.142 75	1.179 21	S0 — ...	1918 ± 6	17.24 ± 0.29	27.4	0.27	41.1	72.8	0.034
3	PGC1179522	224.471 40	0.934 26	S? — E/S0	1887 ± 39	16.90 ± 0.39	48.8	0.54	58.7	90	0.034
4	PGC184851	224.588 25	1.845 33	E-S0 — E	1870 ± 5	15.99 ± 0.29	0.87	0.26	85.6	80	0.041
5	SDSSJ145824.22+020511.0	224.599 95	2.086 30	E — dE	2369 ± 60	–	–	–	–	–	0.037
6	SDSSJ145828.64+013234.6	224.619 30	1.543 03	E — dE,N	1494 ± 20	17.64 ± 0.5	28.1	0.07	154.9	46	0.039
7	PGC1223766	224.670 30	2.339 86	E — dE,N	1559 ± 24	18.36 ± 0.41	15.1	0.07	69.1	45.4	0.036
8	PGC1242097	224.692 05	2.968 99	E — E	1791 ± 40	16.39 ± 0.45	23.9	0.06	129.5	40.3	0.036
9	PGC053521	224.703 00	2.023 50	E — E	1805 ± 2	14.87 ± 0.32	56.0	0.2	2.6	77.5	0.037
10	SDSSJ145944.77+020752.1	224.936 40	2.131 06	E — dE,N	1458 ± 59	18.39 ± 0.5	18.1	0.01	–	16.5	0.035
11	NGC5806	225.001 65	1.891 28	Sb — Scd	1348 ± 3	12.35 ± 0.06	181.2	0.27	172.5	60.4	0.039
12	PGC053587	225.069 15	2.300 69	S0 — S0	1819 ± 3	15.50 ± 0.26	58.6	0.4	10.1	90	0.034
13	SDSSJ150019.17+005700.3	225.080 10	0.950 01	E — dE, N	1961 ± 60	17.56 ± 0.5	28.1	0.07	41.2	44.1	0.042
14	NGC5846:[MTT2005]046	225.112 05	1.475 26	...— pec	1501 ± 60	–	–	–	–	–	0.039
15	NGC5811	225.112 35	1.623 62	SBm — dE	1535 ± 6	14.76 ± 0.32	61.4	0.06	96.8	31.3	0.039
16	SDSSJ150033.02+021349.1	225.137 55	2.230 36	E — dE	1278 ± 37	17.24 ± 0.5	33.0	0.1	31.3	58.2	0.034
17	PGC1193898	225.219 15	1.404 93	E — dE,N	1885 ± 10	16.87 ± 0.39	36.3	0.34	9.6	90	0.038
18	SDSSJ150059.35+015236.1	225.247 05	1.876 70	E — dE,N	2196 ± 48	18.76 ± 0.5	16.1	0.05	96.2	38.1	0.035
19	SDSSJ150059.35+013857.0	225.247 35	1.649 13	E — E	2363 ± 18	18.18 ± 0.35	17.3	0.14	14.7	68.7	0.038
20	SDSSJ150100.85+010049.8	225.253 50	1.013 82	E — dE/I	1737 ± 5	18.03 ± 0.35	23.9	0.21	113.6	90	0.039
21	PGC053636	225.262 95	0.707 64	Sb — S0/a	1724 ± 3	15.88 ± 0.29	32.3	0.11	172.6	40.5	0.043
22	SDSSJ150106.96+020525.1	225.279 00	2.090 31	E — dE,N	1943 ± 25	18.33 ± 0.35	20.8	0.12	154.9	62.3	0.034
23	NGC5813	225.297 00	1.702 01	E — E	1956 ± 7	11.52 ± 0.19	250.1	0.18	142.5	90	0.037
24	PGC1196740	225.313 95	1.498 26	E — dE	2139 ± 5	17.75 ± 0.39	25.1	0.13	0.9	68.3	0.039
25	PGC1205406	225.316 35	1.773 48	E — dE/I	1343 ± 15	18.06 ± 0.45	25.6	0.33	111.5	90	0.036
26	SDSSJ150138.39+014319.8	225.409 95	1.722 04	E — dE,N	2290 ± 15	17.83 ± 0.35	23.9	0.03	–	28.7	0.037
27	PGC1208589	225.410 85	1.870 18	E — dE,N	2152 ± 2	17.90 ± 0.62	14.7	0.09	106.5	52.5	0.034
28	UGC09661	225.514 65	1.841 02	SBd — Sdm	1243 ± 2	14.81 ± 0.3	62.8	0.04	139	28.5	0.034
29	PGC1192611	225.617 40	1.364 22	E — dE	1516 ± 55	18.49 ± 0.47	15.8	0.07	–	45.6	0.036
30	SDSSJ150233.03+015608.3	225.637 50	1.935 82	E — dE/I	1647 ± 60	18.18 ± 0.5	21.8	0.14	17.2	69.2	0.031
31	SDSSJ150236.05+020139.6	225.650 10	2.027 59	E — dE	1992 ± 20	18.11 ± 0.35	30.1	0.42	108.5	90	0.031
32	PGC1230503	225.934 35	2.552 36	E — dE	1782 ± 17	17.56 ± 0.35	20.8	0.14	122.2	69.1	0.032
33	SDSSJ150349.93+005831.7	225.957 90	0.976 51	I — dI	2002 ± 48	16.99 ± 0.5	43.5	0.22	70.8	61.7	0.037
34	PGC1185375	225.959 55	1.126 84	S0 — E	1575 ± 7	16.48 ± 0.35	27.4	0.17	102.8	59.3	0.034
35	PGC087108	225.984 30	0.429 54	I — ...	1581 ± 2	17.32 ± 0.58	26.2	0.15	179.1	50.8	0.032
36	NGC5831	226.029 00	1.219 94	E — E	1631 ± 2	12.44 ± 0.11	134.3	0.05	128.7	38.5	0.034
37	PGC1197513	226.035 15	1.524 54	S0-a — S0/a	1837 ± 2	16.43 ± 0.38	35.7	0.25	11.1	63	0.035
38	PGC1230189	226.054 50	2.542 97	E — E	1909 ± 7	15.89 ± 0.31	42.5	0.15	179.3	73.5	0.029
39	PGC1179083	226.099 35	0.918 39	E — dE	1657 ± 60	18.12 ± 0.5	18.1	0.05	127	38.4	0.034
40	PGC1216386	226.102 95	2.114 62	E — E	1704 ± 13	17.44 ± 0.34	28.1	0.27	97.9	90	0.034
41	NGC5846:[MTT2005]139	226.143 00	1.032 43	E — dE,N	2184 ± 60	–	–	–	–	–	0.034
42	PGC1190315	226.178 70	1.290 88	E — dE	1967 ± 9	16.96 ± 0.42	23.9	0.04	–	33.7	0.032
43	SDSSJ150448.49+015851.3	226.202 25	1.980 84	E — dE	1960 ± 23	18.07 ± 0.5	21.3	0.09	18.3	53.9	0.034
44	PGC1211621	226.268 25	1.964 26	E — E	2381 ± 2	17.60 ± 0.42	16.9	0.07	160.7	45.6	0.034
45	NGC5838	226.359 60	2.099 49	E-S0 — S0	1252 ± 4	11.79 ± 0.12	233.4	0.47	38.8	90	0.029
46	NGC5839	226.364 55	1.634 74	S0 — S0	1227 ± 32	13.69 ± 0.06	86.7	0.05	103.1	30	0.035
47	PGC1190358	226.368 90	1.292 33	I — dE	2304 ± 2	17.79 ± 0.41	28.1	0.1	157.1	41.1	0.037
48	PGC1199471	226.382 55	1.587 72	E — dE,N	919 ± 41	18.15 ± 0.46	17.3	0.1	126.1	56.6	NA
49	PGC1190714	226.407 15	1.303 09	E? — E/dE	2074 ± 17	17.43 ± 0.37	22.3	0.06	114.1	30	0.037
50	PGC1209872	226.460 55	1.908 34	E — dE	1721 ± 9	16.93 ± 0.31	29.4	0.11	177.2	61.1	0.032
51	PGC1213020	226.471 65	2.007 75	I — dI	1300 ± 31	18.35 ± 0.46	21.3	0.27	143.9	67.4	0.032
52	NGC5845	226.503 30	1.633 97	E — E	1450 ± 9	13.44 ± 0.15	60	0.15	152.9	72	0.034
53	PGC1218738	226.514 10	2.184 86	Sm — Sm	1659 ± 4	16.34 ± 0.31	41.5	0.06	148.4	32.6	0.030
54	PGC1191322	226.528 05	1.322 42	E? — E/dE	2300 ± 14	18.01 ± 0.34	19.4	0.21	66	53.5	0.032
55	PGC1215798	226.546 95	2.095 85	Scd — Scd	1824 ± 1	17.64 ± 1.92	51.1	0.68	5.2	82	0.030
56	NGC5846	226.621 80	1.606 29	E — E	1750 ± 32	11.09 ± 0.16	255.9	0.02	–	25	0.035
57	NGC5846A	226.621 50	1.594 94	E — E	2251 ± 18	12.72 ± 0.35	189.7	0.15	111.7	66.7	0.035
58	SDSSJ150634.25+001255.6	226.642 65	0.215 56	E? — ...	2006 ± 75	17.87 ± 0.5	28.7	0.21	22.5	53.3	0.035
59	PGC3119319	226.642 65	1.558 83	E — E	1509 ± 2	16.13 ± 0.35	–	–	140	–	0.035
60	NGC5841	226.645 80	2.004 88	S0-a — S0	1257 ± 2	14.55 ± 0.34	70.5	0.39	152.9	90	0.030
61	PGC1156476	226.670 70	0.076 75	E? — ...	1663 ± 11	18.07 ± 0.32	20.8	0.23	8.9	54.7	0.034

Table 1 – *continued*

Id. No.	Galaxy	RA (J2000) (deg)	Dec. (J2000) (deg)	Morph. type (^{a} — ^{b})	Mean Hel. Vel (km s^{-1})	B_T (mag)	D_{25} (arcsec)	log r_{25}	PA (deg)	Incl. (deg)	$E(B-V)$ (mag)
62	PGC1171244	226.675 20	0.634 45	E — dE	2260 ± 9	17.99 ± 0.28	18.1	0.18	169.7	90	0.033
63	NGC5846:[MTT2005]226	226.743 00	1.994 54	E — dE	1307 ± 60		–	–	–	–	0.030
64	NGC5850	226.781 85	1.544 65	Sb — Sb	2547 ± 3	11.89 ± 0.24	198.7	0.15	114.4	46.9	0.035
65	PGC1185172	226.892 25	1.120 43	S? — E/dE	1586 ± 8	17.64 ± 0.37	19.9	0.16	124	47.7	0.032
66	PGC054004	226.905 00	2.019 54	E —dE,N	1923 ± 10	15.86 ± 0.28	41.5	0.08	–	50.4	0.029
67	NGC5854	226.948 80	2.5686	S0-a — S0	1730 ± 26	12.65 ± 0.09	181.2	0.63	55	90	0.028
68	PGC054016	226.949 10	1.292 09	E — E	2070 ± 7	15.67 ± 0.4	36.1	0.02	–	23.7	0.035
69	PGC1217593	227.005 80	2.151 02	E — E	1073 ± 24	18.04 ± 0.4	19.0	0.15	36.5	76.9	0.027
70	PGC054037	227.023 35	1.651 56	S? — S0/a	1843 ± 3	16.08 ± 0.73	34.5	0.29	115	63.4	0.032
71	NGC5846:[MTT2005]258	227.035 50	2.905 02	E — dE, N	1652 ± 60		–	–	–	–	0.027
72	NGC5846:[MTT2005]259	227.038 35	1.420 58	E — dE, N	2314 ± 60		–	–	–	–	0.032
73	PGC054045	227.038 50	1.608 56	I — dI	2158 ± 21	16.09 ± 0.46	37.8	0.04	–	25.5	0.032
74	SDSSJ150812.35+012959.7	227.051 55	1.499 75	E — dE,N	1537 ± 28	18.02 ± 0.36	22.3	0.01	–	16.6	0.032
75	NGC5846:[MTT2005]264	227.082 75	1.689 63	E — dE,N	2088 ± 60		–	–	–	–	0.029
76	PGC1206166	227.094 45	1.798 48	E — dE, N	1741 ± 13	18.08 ± 0.4	25.6	0.39	139.4	90	0.030
77	NGC5846:[MTT2005]268	227.106 90	1.706 93	E — dE	2049 ± 60		–	–	–	–	0.030
78	PGC1209573	227.196 60	1.9001	E — dE	1991 ± 8	16.67 ± 0.3	41.1	0.36	159.6	90	0.020
79	PGC1176385	227.267 85	0.821 93	Sa — S0/a	1644 ± 2	16.81 ± 0.29	33.7	0.22	179	57.9	0.033
80	SDSSJ150907.83+004329.7	227.282 70	0.724 79	E — dE	1666 ± 10	17.69 ± 0.35	43.5	0.49	133.8	90	0.032
81	PGC1210284	227.312 25	1.921 42	E — dE	1728 ± 9	16.64 ± 0.29	34.5	0.2	87.2	90	0.020
82	NGC5864	227.389 95	3.052 72	S0 — S0	1802 ± 21	12.70 ± 0.19	150.7	0.51	66.5	90	0.027
83	NGC5869	227.455 80	0.470 11	S0 — ...	2074 ± 16	13.15 ± 0.25	131.3	0.19	110.7	61.5	0.032
84	UGC09746	227.570 10	1.933 58	Sbc — Scd	1736 ± 4	14.84 ± 0.27	46.7	0.53	138.6	78.6	0.020
85	UGC09751	227.743 65	1.437 53	Sc — Sd	1553 ± 7	15.97 ± 0.67	73.8	0.58	118.5	78.8	0.027
86	PGC1202458	227.755 50	1.6806	E — dE	1652 ± 18	17.28 ± 0.29	27.4	0.09	171.9	53.1	0.024
87	SDSSJ151121.37+013639.5	227.839 65	1.610 79	E — dE	2029 ± 69	–	–	–	–	–	0.024
88	UGC09760	228.010 50	1.698 49	Scd — Sd	2021 ± 3	15.20 ± 0.65	106.7	0.73	61.2	85.1	0.025
89	PGC1199418	228.034 20	1.585 84	E — E	1941 ± 3	17.00 ± 0.33	20.3	0.07	137.7	45.4	0.025
90	PGC1215336	228.100 05	2.079 99	S? — ...	1684 ± 10	16.94 ± 0.29	30.1	0.19	96.9	50.9	0.015

Notes. [a]Data from HYPERLEDA http://leda.univ-lyon1.fr (Makarov et al. 2014).
[b]Data from Mahdavi et al. (2005).

scheme and values of T as for bright ones. We also added in column 5 the morphological type provided by Mahdavi et al. (2005). These authors identified dwarfs among Ellipticals (Es) distinguishing normal dEs and nucleated dEs,N. Apart from luminosity classification, in very few cases the two morphological classifications differ. Fig. 1 shows the morphological type distribution (top panel) and the apparent B-band magnitudes (bottom panel) of the 90 members of the group. Members with morphological type T ≤ -4 and apparent B magnitudes ≥ 16 dominate.

We compared the members of the group by HYPERLEDA and Mahdavi et al. (2005) selection criteria with those identified in the literature. Mahdavi et al. (2005) argue, on statistical grounds, that a total of 251 ± 10 galaxies, listed in their table 1 composed of 324 candidates, are members of the group. In their table 2, Mahdavi et al. (2005) provide the number of spectroscopically confirmed members, which amount to 84, belonging to different classes statistically established. These classes range from 0 to 5, i.e. from members confirmed by spectroscopy, priority rating 0, to galaxies excluded by their statistical surface brightness criteria, priority rating 5. Our selection of 90 members includes all 84 spectroscopically confirmed members of Mahdavi et al. (2005), four dwarfs with spectroscopic redshift included in the Eigenthaler & Zeilinger (2010) list, plus other two ETGs in HYPERLEDA. We report in column 3 of Table 3 the identification number provided by Mahdavi et al. (2005) and by Eigenthaler & Zeilinger (2010). All dwarfs in the Eigenthaler & Zeilinger (2010) list, but two, NGC 5486_56 and NGC 5846_51, are included by our selection criteria. PGC087108 according to Eigenthaler & Zeilinger (2010) are two H II regions classified as individual galaxies in SDSS e in Principal Galaxy Catalogue (PGC). UV imaging indicated that it is a galaxy (see Section 4.1).

Summarizing, our selection procedure includes all spectroscopically confirmed members present in the Mahdavi et al. (2005) and Eigenthaler & Zeilinger (2010) lists within a diameter of ∼1.5 Mpc about the group centre. As explained in the following section, we extended the search of spectroscopic possible members in a wider area of 4 Mpc. Additional galaxies, not included in Mahdavi et al. (2005) and Eigenthaler & Zeilinger (2010), with a redshift measure are listed in Table B1. Although compatible with membership in the redshift space, they are distant from the centre of mass of the group and outside the box of 1.8 Mpc considered by Mahdavi et al. (2005).

2.2 Substructures

The presence of substructures in a galaxy group is a signature of recent accretion and therefore probes the evolution of its members (e.g Firth et al. 2006; Hou et al. 2012). Substructures manifest as a deviation in the spatial and/or velocity arrangement of the system.

If a group is a dynamically relaxed system, the spatial distribution of its galaxies should be approximately spherical and their velocity distribution Gaussian. The presence of substructures indicates a departure from this quasi-equilibrium state. As already discussed in Paper II, at least one of the following characteristics

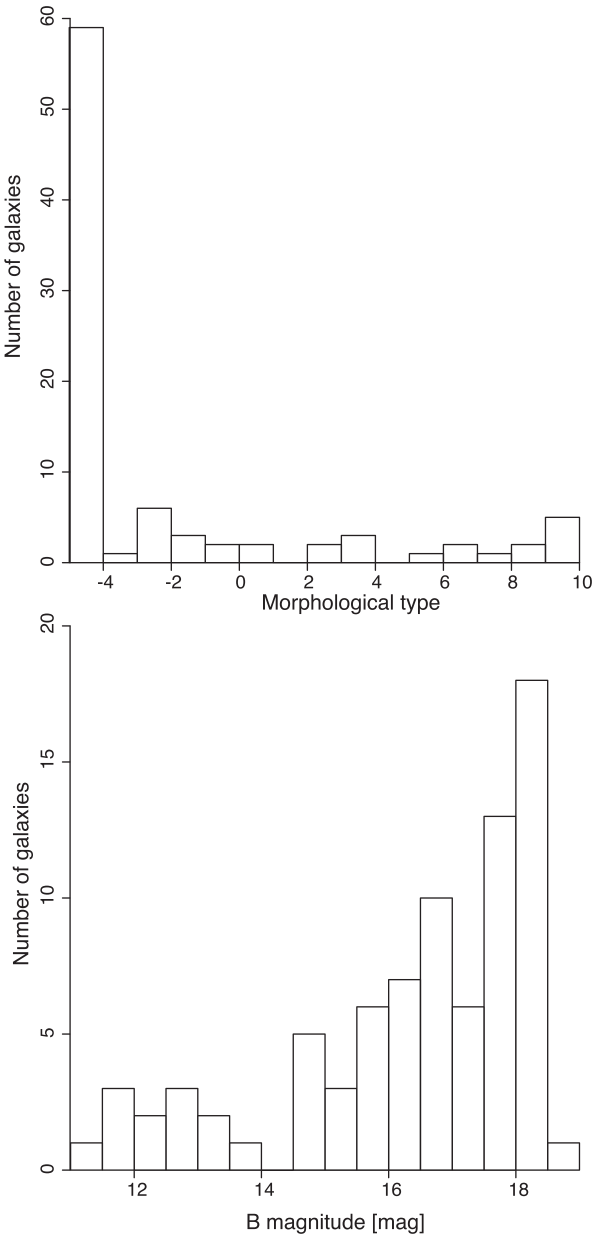

Figure 1. Morphological type (top) and B magnitude (bottom) distributions of NGC 5846 members from HYPERLEDA. All members are spectroscopically confirmed (see Section 2).

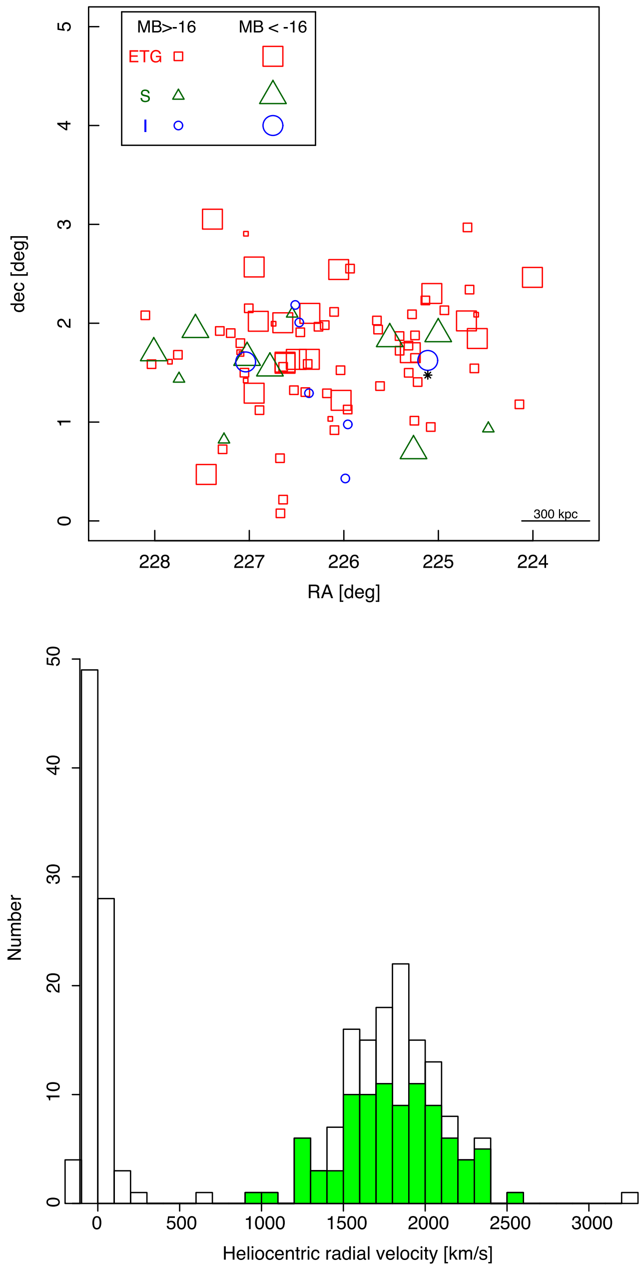

Figure 2. Top: spatial distribution of galaxy members separated in B-magnitude bins and morphological type. The smallest symbols are galaxies with no B magnitudes. Black asterisk refer to galaxies with no B magnitudes and no morphological types. Bottom: histogram of the heliocentric radial velocity (10–3000 km s^{-1}) of galaxies within a box of 4 Mpc^2 centred on NGC 5846. The width of the velocity bins is 100 km s^{-1}. Green filled bins show the velocity distribution of the 90 members listed in Table 1.

shows the presence of substructures: (i) significant multiple peaks in the galaxy position distribution; (ii) significant departures from a single-Gaussian velocity distribution; (iii) correlated deviations from the global velocity and position distribution.

Fig. 2 shows the projected spatial distribution of the group members (top panel). Galaxies are separated in B-magnitude bins and morphological types. ETGs, Spirals, and Irregulars, with absolute magnitudes $M_B > -16$ and, $M_B < -16$ are indicated with squares, triangles, and circles of increasing size, respectively. The group is dominated by ETGs (72 per cent), 60 per cent Ellipticals[1] approximately homogeneously distributed. Two peaks may be present in the projected spatial distribution.

The velocity distribution of group members is shown in Fig. 2 (bottom panel, filled bins). To discern if the heliocentric radial velocity has a Gaussian distribution, we applied the Anderson–Darling normality test and found it does not significantly depart (p-value = 0.92) from normality.

We also performed the Dressler & Shectman (1988) test (DS test hereafter), which uses both spatial information and velocity, to find substructures in our group. The DS test identifies a fixed number, NN, of nearest neighbours on the sky around each galaxy, computes the local mean velocity and velocity dispersion of this subsample,

[1] Morphological type ≤ -3.

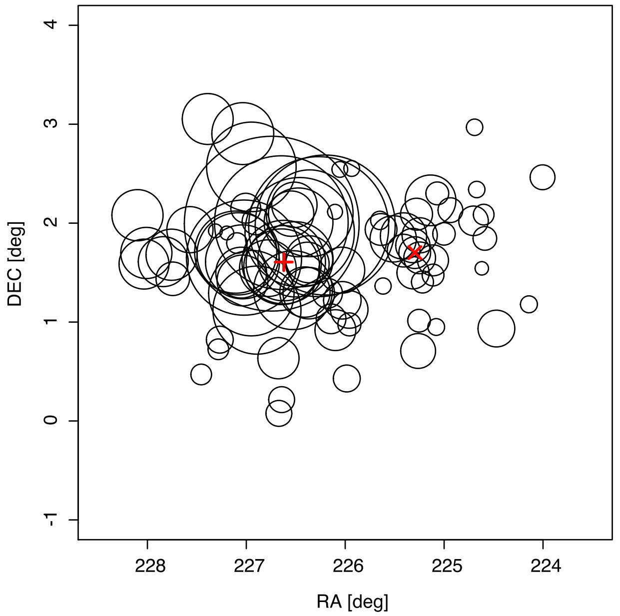

Figure 3. DS 'bubble-plot' based on the 10 nearest galaxies. The bubble size is proportional to the squared deviation of the local velocity distribution from the group velocity distribution. Red plus and cross show the position of NGC 5846 and NGC 5813, respectively.

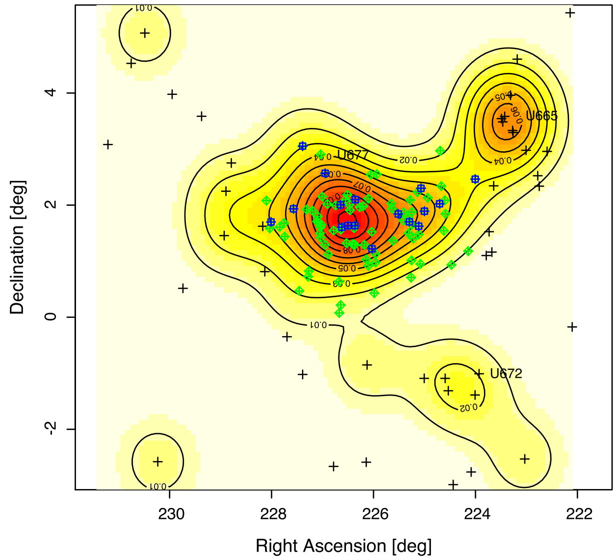

Figure 4. Spatial distribution of galaxies within a box of 4×4 Mpc^2 centred on NGC 5846 (shaded yellow/red area). Blue squares show the members of the group listed in the catalogue of Ramella et al. (2002) and green diamonds indicate the added members (Section 2). The map is normalized to the total density. The 2D binned kernel-smoothed number density contours for the galaxies with $m_B \leq 15.5$ mag (circle + cross) are shown. The value of $m_B = 15.5$ mag is the magnitude limit of the Ramella et al. (2002) catalogue.

and compares these values with the average velocity and velocity dispersion of the entire group, $\bar{v}$ and $\sigma_{\rm gr}$, respectively. The deviations of the local average velocity and the dispersions from the global values are summed. In particular, for the galaxy i, the deviation of its projected neighbours is defined as $\delta_i = ({\rm NN}+1)/\sigma_{\rm gr}\ [\ (v_{\rm loc} - \bar{v})^2 + (\sigma_{\rm loc} - \sigma)^2]$, where $v_{\rm loc}$ and $\sigma_{\rm loc}$ are the local average velocity and velocity dispersion. The total deviation, Δ, is the sum of the local deviations, $\delta_i : \Delta = \sum_i^N \delta_i$, where N is the number of the group members. If the group velocity distribution is close to Gaussian and the local variations are only random fluctuations, Δ will be of the order of N. If Δ varies significantly from N then there is probable substructure.

To compute δ, we set the number of neighbours, NN, at $10 \approx N^{1/2}$ (see e.g. Silverman 1986). Since δ_i are not statistically independent, it is necessary to calibrate the Δ statistic by performing a Monte Carlo analysis. The velocities are randomly shuffled among the positions and $\Delta_{\rm sim}$ is recomputed 10 000 times to provide the probability that the measured Δ is a random result. The significance of having substructure, given by the p-value, is quantified by the ratio of the number of the simulations in which the value of $\Delta_{\rm sim}$ is larger than the observed value, and the total number of simulations: $p = (N(\Delta_{\rm sim} > \Delta)/N_{\rm sim})$.

It should be noted that the Δ statistic is insensitive to subgroups that are well superimposed. It relies on some displacement of the centroids of the subgroups.

The p-value measures the probability that a value of $\Delta_{\rm sim} \geq \Delta$ occurs by chance; a p-value > 0.10 gives a high significance level to the presence of substructures, values ranging from 0.01 and 0.10 give substructures from marginal to probable.

In Fig. 3, we show the DS 'bubble-plot'; each galaxy in the group is marked by a circle whose diameter scales with e^{δ}. Larger circles indicate larger deviations in the local kinematics compared to the global one. Many large circles in an area indicate a correlated spatial and kinematical variation, i.e. a substructure. We also show the position of NGC 5846 and NGC 5813. The group does not present significant substructures ($p = 0.07$).

2.3 Group's environment density analysis

In order to characterize the environment of the group, we have considered the galaxy distribution within a box of 4×4 Mpc^2 (about two times the size of a typical group) centred on NGC 5846. From the HYPERLEDA data base, we have selected all the galaxies within such box with a heliocentric radial velocity within $\pm 3\sigma$ of the group mean velocity, as given in the catalogue of Ramella et al. (2002). We have found 136 galaxies (Table 1 and Table B1 in Appendix B). In the bottom panel of Fig. 2, we highlight the velocity distribution of group members (green filled bins) given in Table 1 superposed on that of galaxies in the 4×4 Mpc^2 box. Among these galaxies, we have selected only those more luminous than 15.5 mag in the B band (i.e. the magnitude limit of the galaxies in Ramella et al. (2002), and on this sample we performed a density analysis. The 2D binned kernel-smoothed number density contour map is shown in Fig. 4. Density in the 4×4 Mpc^2 box (shaded yellow) is colour coded. The highest densities correspond to the red regions; in the normalized map, density levels above 0.05 are in yellow. Blue squares show the members of the group from the catalogue of Ramella et al. (2002) and green diamonds indicate the new members that we have added (as explained in Section 2.1).

A high-density region approximately centred on NGC 5846, and elongated towards NGC 5813, the second B-band brighter member, appears. There are also two poor groups, USGC U665 and USGC U672, likely falling towards NGC 5846.

2.4 Group dynamical properties

The virial theorem provides the standard method to estimate the mass of a self-gravitating system from dynamical parameters,

Table 2. Kinematical and dynamical properties of NGC 5846.

Group name	Centre of mass RA (deg) Dec.	V_{group} (km s^{-1})	Velocity dispersion (km s^{-1})	D (Mpc)	Harmonic radius (Mpc)	Virial mass (10^{13} M$_{\odot}$)	Projected mass (10^{13} M$_{\odot}$)	Crossing time × H_0
NGC 5846	226.185 01 1.653 21	1798^{+8}_{-10}	327^{+12}_{-2}	$24.0^{+0.1}_{-0.1}$	$0.35^{+0.01}_{-0.01}$	$4.15^{+0.24}_{-0.16}$	$8.24^{+0.56}_{-0.13}$	$0.12^{+0.00}_{-0.01}$
NGC5846^a	226.761 39 1.650 59	1800^{+13}_{-15}	332^{+18}_{-3}	$24.0^{+0.2}_{-0.2}$	$0.27^{+0.01}_{-0.01}$	$3.24^{+0.29}_{-0.20}$	$5.42^{+0.43}_{-0.13}$	$0.09^{+0.01}_{-0.00}$

Note. ^{a}The same quantities computed excluding the first 30 galaxies in Table 1, i.e. NGC 5813 and its surroundings.

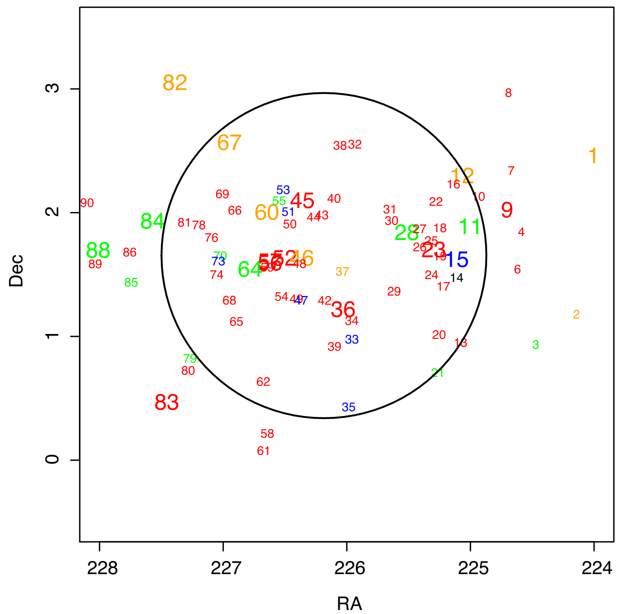

Figure 5. Projected distribution of the galaxy members of the NGC 5846 group. Numbers refer to their identification in Table 1. Different morphological types correspond to different colours as in Fig. 2. Galaxies with B magnitude $\leq$ 15.5 are labelled with bigger numbers than those with B magnitude > 15.5 or unknown (in black). The circle (solid line) centred on the centre of mass of the group encloses galaxies within the virial radius of 550 kpc.

positions and velocities of the group members. It applies if the system analysed is in dynamical equilibrium and its luminosity is a tracer of the mass.

We derived the kinematic and dynamical properties of NGC 5846, following the approach described in Firth et al. (2006, their table 6) and already used in Paper I for LGG 225 and Marino et al. (2014) for USGC U268 and USGC U376.

Results are summarized in Table 2. The errors have been computed via jackknife simulations (e.g. Efron 1982). In order to obtain an estimate of the compactness of the group, we computed the harmonic mean radius using the projected separations r_{ij} between the i-th and j-th group member. Fig. 5 shows the relative positions of the group members with superposed a circle centred on the centre of mass of the group and radius corresponding to the virial radius.

The projected mass is about two times the virial mass. The contribution of the 30 galaxies surrounding NGC 5813 (Table 1) is about 20 per cent of the virial mass and 34 per cent of the projected one (see the second line in Table 2).

For comparison, the projected mass of the groups USGC 268 and USGC U376 (Marino et al. 2014), is a factor 3–4 times the virial one. Using N-body simulations, Perea, del Olmo & Moles (1990) showed that the virial mass estimate is better than the projected mass estimate since it is less sensitive to anisotropies or subclustering. However, it may be affected by the presence of interlopers, i.e. unbound galaxies, and by a mass spectrum. Both factors would cause an overestimation of the group mass. Therefore, the estimated masses are upper limits. Another caveat concerning the virial mass is that the groups may not be virialized (e.g. Ferguson & Sandage 1990).

The larger difference in the virial and projected mass estimates of USGC U268 and USGC U376 may suggest a larger probability of interlopers, although these groups are, on average, closer than NGC5846 group (15 and 19 Mpc, respectively; Marino et al. 2014), or that these are not yet virialized.

The crossing time is usually compared to the Hubble time to determine whether the groups are gravitationally bound systems. The derived crossing time of NGC 5846 group (see Table 2) suggests that it could be virialized (e.g. Firth et al. 2006).

3 OBSERVATIONS AND DATA REDUCTION

3.1 UV and optical data

The UV imaging was obtained from *GALEX* (Martin et al. 2005; Morrissey et al. 2007) GI programme 017 (PI A. Marino) and archival data in two ultraviolet bands, FUV (1344–1786 Å) and NUV (1771–2831 Å). The instrument has a very wide field of view (1°.25 diameter) and a spatial resolution of ≈4.2 and 5.3 arcsec full width at half-maximum in FUV and NUV, respectively, sampled with 1.5 arcsec × 1.5 arcsec pixels (Morrissey et al. 2007).

We used only UV images having a distance from the centre of the field of view ≤0.5 deg, as generally the photometric quality is better in the central part of the field (Bianchi et al. 2011; Bianchi 2014). In case of multiple observations of the same galaxy, we chose the one with longer exposure time.

This yields *GALEX* data for 78 of the 90 member galaxies, of which all but four (UGC09746, PGC1202458, SDSSJ151121.37+013639.5, PGC1199418) were observed in both FUV and NUV (see Table 2).

The exposure times (see Table 3) for most of our sample are ∼2000 s (limit AB magnitude in FUV/NUV of ∼22.6/22.7; Bianchi 2009). We used FUV and NUV intensity images to compute integrated photometry of the galaxies and light profiles, as described in Section 4.

In addition, we used optical SDSS archival data in the u [2980–4130 Å], g [3630–5830 Å], r [5380–7230 Å], i [6430–8630 Å], and z [7730–11230 Å] filters (Adelman-McCarthy et al. 2008) to obtain optical photometry.

3.2 Aperture photometry

UV and optical magnitudes of the brighter members ($B_T \leq$ 15.5 mag) have been obtained as follows.

The UV and optical surface photometry was carried out using the ELLIPSE fitting routine in the STSDAS package of IRAF

Table 3. The NGC 5846 group members and the journal of the UV observations with *GALEX*.

Id No.	Galaxy	MTT05	*P*	NUV Exp. Time (s)	FUV Exp. Time (s)	Survey
1	PGC053384	–	–	1602.1	1602.1	MIS
2	PGC1186917	–	–	1640.7	1640.7	MIS
3	PGC1179522	009	0	1640.7	1640.7	MIS
4	PGC184851	013	2	1648.0	162.0	GI6 AIS
5	SDSS J145824.22+020511.0	014	1	1648.0	162.0	GI6 AIS
6	SDSSJ145828.64+013234.6	017	2	1640.7	1640.7	MIS
7	PGC1223766	018	3	1648.0	162.0	GI6 AIS
8	PGC1242097	020	5	2107.5	2107.5	MIS
9	PGC053521	021	0	1648.0	162.0	GI6 AIS
10	SDSSJ145944.77+020752.1	030	2	1648.0	162.0	GI6 AIS
11	NGC5806	037	0	2521.2	2521.2	GI3
12	PGC053587	042	0	1648.0	162.0	GI6 AIS
13	SDSSJ150019.17+005700.3	045	1	335.0	159.0	AIS
14	NGC 5846:[MTT2005] 046	046	0	2521.2	2521.2	GI3
15	NGC5811	047	3	2521.2	2521.2	GI3
16	SDSSJ150033.02+021349.1	048	1	1648.0	162.0	GI6 AIS
17	PGC1193898	055	2	2521.2	2521.2	GI3
18	SDSSJ150059.35+015236.1	058	2	2521.2	2521.2	GI3
19	SDSSJ150059.35+013857.0	059	5	2521.2	2521.2	GI3
20	SDSSJ150100.85+010049.8	060	2	335.0	159.0	AIS
21	PGC053636[a]	061	0			
22	SDSSJ150106.96+020525.1	063	2	2521.2	2521.2	GI3
23	NGC5813	064	0	2521.2	2521.2	GI3
24	PGC1196740	068	2	2521.2	2521.2	GI3
25	PGC1205406	069	3	2521.2	2521.2	GI3
26	SDSSJ150138.39+014319.8	073	2	2521.2	2521.2	GI3
27	PGC1208589	075	3	2521.2	2521.2	GI3
28	UGC09661	083	0	2521.2	2521.2	GI3
29	PGC1192611	088	3	5299.3	2359.1	GI1
30	SDSSJ150233.03+015608.3	090	1	2521.2	2521.2	GI3
31	SDSSJ150236.05+020139.6	091	3	2521.2	2521.2	GI3
32	PGC1230503	113	3	2399.4	2399.4	MIS
33	SDSSJ150349.93+005831.7	114	0	5299.3	2359.1	GI1
34	PGC1185375	115	0	5299.3	2359.1	GI1
35	PGC087108	$NGC5846_{41/42}$	Eigenthaler	1692.0	1692.0	MIS
36	NGC5831	122	0	5299.3	2359.1	GI1
37	PGC1197513	124	0	5299.3	2359.1	GI1
38	PGC1230189	125	3	2399.4	2399.4	MIS
39	PGC1179083	131	2	5299.3	2359.1	GI1
40	PGC1216386	132	3	2399.4	2399.4	MIS
41	SDSSJ150434.31+010156.9	139	1	5299.3	2359.1	GI1
42	PGC1190315	142	0	5299.3	2359.1	GI1
43	SDSSJ150448.49+015851.3	144	2	2399.4	2399.4	MIS
44	PGC1211621	148	0	2399.4	2399.4	MIS
45	NGC5838	159	0	2399.4	2399.4	MIS
46	NGC5839	160	0	2484.2	2484.2	MIS
47	PGC1190358	162	0	5299.3	2359.1	GI1
48	PGC1199471	165	3	2484.2	2484.2	MIS
49	PGC1190714	167	0	2484.2	2484.2	MIS
50	PGC1209872	177	0	1466.0	1466.0	GI3
51	PGC1213020	180	3	1466.0	1466.0	GI3
52	NGC5845	184	0	2484.2	2484.2	MIS
53	PGC1218738	187	2	1466.0	1466.0	GI3
54	PGC1191322	191	0	2484.2	2484.2	MIS
55	PGC1215798	192	0	1466.0	1466.0	GI3
56	NGC5846A	201	0	2484.2	2484.2	MIS
57	NGC5846	202	0	2484.2	2484.2	MIS
58	SDSSJ150634.25+001255.6	$NGC5846_{44}$	Eigenthaler	1695.1	1694.1	MIS
59	PGC3119319	205	5	2484.2	2484.2	MIS
60	NGC5841	206	0	1466.0	1466.0	GI3
61	PGC1156476	$NGC5846_{50}$	Eigenthaler	164.0	164.0	AIS

Table 3 – *continued*

Id No.	Galaxy	MTT05	*P*	NUV Exp. Time (s)	FUV Exp. Time (s)	Survey
62	PGC1171244	212	3	1695.1	1694.1	MIS
63	SDSS J150658.37+015939.5	226	2	1466.0	1466.0	GI3
64	NGC5850	233	0	2484.2	2484.2	MIS
65	PGC1185172	241	3	163.0	163.0	AIS
66	PGC054004	244	0	2376.0	2375.0	MIS
67	NGC5854	246	0	2376.0	2375.0	MIS
68	PGC054016[a]	247	0			
69	PGC1217593	252	5	2376.0	2375.0	MIS
70	PGC054037[b]	256	4			
71	SDSSJ150808.43+025416.5	258	3	2376.0	2375.0	MIS
72	NGC5846:[MTT2005]259[b]	259	3			
73	PGC054045[b]	260	0			
74	SDSSJ150812.35+012959.7[b]	261	3			
75	NGC 5846:[MTT2005][b]	264	2			
76	PGC1206166[b]	266	2			
77	SDSSJ150825.57+014224.8[b]	268	2	–		
78	PGC1209573[a]	276	3			
79	PGC1176385	283	0	1696.0	1696.0	MIS
80	SDSSJ150907.83+004329.7	287	2	1696.0	1696.0	MIS
81	PGC1210284[a]	290	3			
82	NGC5864[b]	299	0			
83	NGC5869	NGC5869	Eigenthaler	1450.6	1450.6	MIS
84	UGC09746	305	0	1655.0	[a]	GI6
85	UGC09751	311	0	1696.0	1696	MIS
86	PGC1202458	313	2	1655.0	[a]	GI6
87	SDSSJ151121.37+013639.5	317	1	1655.0	[b]	GI6
88	UCG09760	321	0	1655.0	111.0	GI6 AIS
89	PGC1199418	323	5	1655.0	[a]	GI6
90	PGC1215336	$NGC5846_{52}$	Eigenthaler	2905.9	1732.3	MIS

Notes. Column 1 and column 2: galaxy identification; column 3 and column 4: galaxy identification and membership probability in Mahdavi et al. (2005), Table 1, respectively. *P* values are: 0, no-SDSS spectroscopic redshift; 1, probable member; 2, possible member; 3, conceivable member; 4 and 5 likely not a member.
[a]The UV images have a distance from the centre of the field of view >50 arcmin.
[b]There are no FUV *GALEX* images for these galaxies.

(Jedrzejewski 1987). The SDSS images (corrected frames with the soft bias of 1000 counts subtracted) in the five bands were registered to the corresponding *GALEX* NUV intensity images before evaluating brightness profiles, using the IRAF tool `register`. We masked the foreground stars and the background galaxies in the regions where we measured the surface brightness profiles. To secure a reliable background measure, we forced the measure of five isophotes well beyond the galaxy emission.

From the surface brightness profiles, we derived total apparent magnitudes as follows. For each profile, we computed the integrated apparent magnitude within elliptical isophotes up to the radius where the mean isophotal intensity is 2σ above the background. The background was computed around each source, as the mean of sky value of the outer five isophotes. Errors of the UV and optical magnitudes where estimated by propagating the statistical errors on the mean isophotal intensity provided by ELLIPSE. In addition to the statistical error, we added systematic uncertainties in the zero-point calibration of 0.05 and 0.03 mag in FUV and NUV, respectively (Morrissey et al. 2007). Surface photometry was corrected for galactic extinction assuming Milky Way dust properties with $R_v = 3.1$ (Cardelli, Clayton & Mathis 1989), $A_{\rm FUV}/E(B-V) = 8.376$, $A_{\rm NUV}/E(B-V) = 8.741$, and $A_r/E(B-V) = 2.751$.

Table 4 lists the measured AB magnitudes both in UV and optical[2] bands, uncorrected for foreground Galaxy extinction. UV and optical magnitudes of fainter members were extracted from the *GALEX* and SDSS pipelines. We used the FUV and NUV calibrated magnitudes and the Model magnitudes[3] from the *GALEX* and SDSS pipelines, respectively.

4 RESULTS

Hereafter, following the definition of Tammann (1994), we considered as dwarfs galaxies fainter than $M_B = -16$ mag ($M_V = -17$ mag), and as ETGs, galaxies with morphological type T ≤ 0 (i.e E-S0a-dE-dE,N-dS0) as in Boselli & Gavazzi (2014).

4.1 UV versus optical morphological classification

Table 1 (column 5) compares the morphological classification of members we adopted with that in Mahdavi et al. (2005). In Appendix A, we show the UV (left-hand panels) and SDSS

[2] We converted SDSS counts to magnitudes following the recipe provided in http://www.sdss.org/df7/algorithms/fluxcal.html.
[3] http://www.sdss.org/dr5/algorithms/photometry.html

Table 4. UV and optical photometry of the galaxy group.

Id. No.	Galaxy	FUV (AB mag)	NUV (AB mag)	*u* (AB mag)	*g* (AB mag)	*r* (AB mag)	*i* (AB mag)	*z* (AB mag)
1	PGC053384	20.520 ± 0.090	18.740 ± 0.040	16.250 ± 0.010	14.670 ± 0.010	14.080 ± 0.010	13.7501 ± 0.010	13.700 ± 0.010
2	PGC1186917	23.678 ± 0.405	21.039 ± 0.100	18.449 ± 0.058	16.911 ± 0.006	16.236 ± 0.005	15.901 ± 0.005	15.684 ± 0.014
3	PGC1179522	21.368 ± 0.113	20.067 ± 0.062	17.991 ± 0.040	16.470 ± 0.006	15.761 ± 0.005	15.453 ± 0.006	15.235 ± 0.014
4	PGC184851	21.851 ± 0.370	19.926 ± 0.115	17.431 ± 0.025	15.806 ± 0.003	15.040 ± 0.003	14.670 ± 0.003	14.362 ± 0.009
5	SDSSJ145824.22+020511.0		21.629 ± 0.220	20.339 ± 0.482	18.913 ± 0.046	18.425 ± 0.049	18.388 ± 0.070	18.136 ± 0.265
6	SDSSJ145828.64+013234.6	20.617 ± 0.090	19.668 ± 0.048	19.227 ± 0.165	17.397 ± 0.012	16.751 ± 0.010	16.446 ± 0.011	16.238 ± 0.038
7	PGC1223766		21.924 ± 0.292	19.372 ± 0.131	17.886 ± 0.015	17.201 ± 0.012	16.885 ± 0.015	16.848 ± 0.064
8	PGC1242097	18.504 ± 0.013	17.970 ± 0.009	16.796 ± 0.010	15.769 ± 0.003	15.372 ± 0.003	15.159 ± 0.003	15.018 ± 0.006
9	PGC053521		18.900 ± 0.040	15.920 ± 0.010	14.330 ± 0.010	13.620 ± 0.010	13.220 ± 0.010	13.080 ± 0.010
10	SDSSJ145944.77+020752.1		21.650 ± 0.273	19.271 ± 0.139	18.114 ± 0.018	17.519 ± 0.017	17.193 ± 0.022	17.113 ± 0.096
11	NGC5806	15.830 ± 0.050	15.180 ± 0.030	13.600 ± 0.010	11.990 ± 0.010	11.320 ± 0.010	10.860 ± 0.010	10.600 ± 0.010
12	PGC053587		19.240 ± 0.040	16.870 ± 0.010	15.140 ± 0.010	14.440 ± 0.010	14.020 ± 0.010	13.950 ± 0.010
13	SDSSJ150019.17+005700.3		21.101 ± 0.267	18.957 ± 0.113	17.303 ± 0.010	16.597 ± 0.009	16.306 ± 0.010	16.158 ± 0.031
14	NGC5846:[MTT2005]046	23.516 ± 0.354	23.311 ± 0.376					
15	NGC5811	17.310 ± 0.050	16.780 ± 0.030	15.620 ± 0.010	14.450 ± 0.010	13.810 ± 0.010	13.350 ± 0.010	13.400 ± 0.010
16	SDSSJ150033.02+021349.1		21.365 ± 0.269	18.510 ± 0.098	16.979 ± 0.009	16.306 ± 0.008	16.038 ± 0.011	16.588 ± 0.089
17	PGC1193898		20.438 ± 0.093	18.004 ± 0.061	16.410 ± 0.006	15.691 ± 0.005	15.339 ± 0.006	15.136 ± 0.022
18	SDSSJ150059.35+015236.1		21.946 ± 0.186	19.614 ± 0.152	18.506 ± 0.022	17.840 ± 0.020	17.568 ± 0.026	17.496 ± 0.104
19	SDSSJ150059.35+013857.0		23.147 ± 0.403	19.598 ± 0.189	17.968 ± 0.017	17.216 ± 0.015	16.814 ± 0.014	16.528 ± 0.043
20	SDSSJ150100.85+010049.8	21.456 ±0.333	20.303 ± 0.125	18.980 ± 0.110	17.800 ± 0.020	17.394 ± 0.018	17.487 ± 0.072	17.126 ± 0.093
21	PGC053636			16.888 ± 0.012	15.640 ± 0.003	15.004 ± 0.003	14.691 ± 0.003	14.460 ± 0.006
22	SDSSJ150106.96+020525.1		22.252 ± 0.198	19.840 ± 0.245	18.069 ± 0.020	17.350 ± 0.018	17.124 ± 0.020	16.935 ± 0.074
23	NGC5813	17.910 ±0.050	16.330 ± 0.030	13.320 ± 0.010	11.450 ± 0.010	10.500 ± 0.010	10.140 ± 0.010	9.880 ± 0.010
24	PGC1196740	20.898 ± 0.068	19.991 ± 0.049	18.531 ± 0.076	17.315 ± 0.010	16.851 ± 0.011	16.595 ± 0.013	16.473 ± 0.042
25	PGC1205406	22.333 ± 0.153	21.003 ± 0.110	18.954 ± 0.101	17.612 ± 0.013	17.006 ± 0.022	16.745 ± 0.026	16.678 ± 0.062
26	SDSSJ150138.39+014319.8		21.898 ± 0.262	19.030 ± 0.110	17.583 ± 0.012	16.877 ± 0.011	16.482 ± 0.012	16.589 ± 0.056
27	PGC1208589	22.332 ± 0.136	21.662 ± 0.111	18.549 ± 0.085	17.259 ± 0.011	16.691 ± 0.011	16.429 ± 0.015	16.168 ± 0.045
28	UGC09661	16.690 ± 0.050	16.420 ± 0.030	15.190 ± 0.010	14.230 ± 0.010	14.040 ± 0.010	13.280 ± 0.010	13.670 ± 0.010
29	PGC1192611		21.618 ± 0.094	19.423 ± 0.149	17.909 ± 0.018	17.349 ± 0.021	17.103 ± 0.032	17.063 ± 0.116
30	SDSSJ150233.03+015608.3	22.248 ± 0.141	21.389 ± 0.106	19.425 ± 0.209	17.918 ± 0.027	17.294 ± 0.021	17.074 ± 0.039	17.015 ± 0.096
31	SDSSJ150236.05+020139.6		21.659 ± 0.146	19.897 ± 0.205	17.854 ± 0.014	17.196 ± 0.016	16.876 ± 0.016	16.824 ± 0.052
32	PGC1230503	23.826 ± 0.619		18.591 ± 0.076	17.157 ± 0.010	16.491 ± 0.007	16.202 ± 0.010	15.991 ± 0.027
33	SDSSJ150349.93+005831.7	18.110 ± 0.018	17.644 ± 0.007	17.938 ± 0.050	16.744 ± 0.009	16.430 ± 0.011	16.058 ± 0.012	15.805 ± 0.032
34	PGC1185375	23.627 ± 0.484	19.915 ± 0.050	17.670 ± 0.040	16.002 ± 0.004	15.247 ± 0.003	14.865 ± 0.004	14.598 ± 0.008
35	PGC087108	17.170 ± 0.013	17.073 ± 0.008	17.571 ± 0.041	16.622 ± 0.008	16.404 ± 0.010	16.449 ± 0.017	16.427 ± 0.052
36	NGC5831	18.900 ± 0.060	17.150 ± 0.030	14.070 ± 0.010	12.110 ± 0.010	11.300 ± 0.010	10.860 ± 0.010	10.630 ± 0.010
37	PGC1197513	19.675 ± 0.035	18.845 ± 0.014	17.190 ± 0.030	15.932 ± 0.004	15.413 ± 0.005	15.169 ± 0.006	15.052 ± 0.018
38	PGC1230189		19.916 ± 0.058	17.214 ± 0.032	15.565 ± 0.005	14.853 ± 0.004	14.473 ± 0.005	14.308 ± 0.014
39	PGC1179083	23.494 ± 0.506		19.196 ± 0.114	17.358 ± 0.011	16.680 ± 0.013	16.516 ± 0.017	16.409 ± 0.033
40	PGC1216386	23.282 ± 0.282	20.920 ± 0.099	18.466 ± 0.057	17.006 ± 0.007	16.362 ± 0.007	16.044 ± 0.007	15.828 ± 0.025
41	NGC5846:[MTT2005]139		22.596 ± 0.241	19.619 ± 0.149	18.534 ± 0.032	17.808 ± 0.022	17.564 ± 0.028	17.346 ± 0.085
42	PGC1190315		20.907 ± 0.068	18.222 ± 0.095	16.485 ± 0.006	15.775 ± 0.005	15.386 ± 0.008	15.207 ± 0.020
43	SDSSJ150448.49+015851.3	21.178 ± 0.085	20.263 ± 0.071	18.979 ± 0.126	17.818 ± 0.018	17.275 ± 0.021	17.098 ± 0.027	17.033 ± 0.089
44	PGC1211621	19.296 ± 0.028	18.954 ± 0.016	17.987 ± 0.031	17.110 ± 0.006	16.671 ± 0.007	16.545 ± 0.009	16.502 ± 0.032
45	NGC5838	18.290 ± 0.050	16.700 ± 0.030	13.320 ± 0.010	11.520 ± 0.010	10.710 ± 0.010	10.240 ± 0.010	9.980 ± 0.010
46	NGC5839	19.420 ± 0.060	18.010 ± 0.030	14.620 ± 0.010	12.930 ± 0.010	12.100 ± 0.010	11.690 ± 0.010	11.400 ± 0.010
47	PGC1190358	19.199 ± 0.029	18.794 ± 0.013	18.308 ± 0.073	17.933 ± 0.018	17.612 ± 0.022	17.651 ± 0.038	18.249 ± 0.254
48	PGC1199471		21.734 ± 0.159	19.198 ± 0.124	17.612 ± 0.012	16.938 ± 0.012	16.641 ± 0.012	16.456 ± 0.074
49	PGC1190714	23.202 ± 0.302	20.520 ± 0.087	18.466 ± 0.063	17.004 ± 0.008	16.350 ± 0.006	16.018 ± 0.007	15.908 ± 0.024
50	PGC1209872	23.082 ± 0.399	21.006 ± 0.120	18.402 ± 0.076	16.593 ± 0.006	15.860 ± 0.005	15.518 ± 0.005	15.308 ± 0.019
51	PGC1213020	19.849 ± 0.053	19.574 ± 0.037	18.599 ± 0.074	17.817 ± 0.014	17.448 ± 0.025	17.337 ± 0.049	17.422 ± 0.103
52	NGC5845	19.470 ± 0.060	18.290 ± 0.030	14.860 ± 0.010	12.990 ± 0.010	12.150 ± 0.010	11.710 ± 0.010	11.430 ± 0.010
53	PGC1218738	18.268 ± 0.025		17.104 ± 0.034	15.912 ± 0.008	15.464 ± 0.014	15.441 ± 0.028	15.092 ± 0.039
54	PGC1191322		21.423 ± 0.142	19.157 ± 0.084	17.625 ± 0.009	16.944 ± 0.008	16.621 ± 0.010	16.417 ± 0.029
55	PGC1215798	17.434 ± 0.016	17.182 ± 0.011	17.101 ± 0.022	16.283 ± 0.005	16.055 ± 0.006	16.005 ± 0.008	15.854 ± 0.035
56	NGC5846+A	17.050 ± 0.050	16.060 ± 0.030	12.460 ± 0.010	10.570 ± 0.010	9.770 ± 0.010	9.300 ± 0.010	9.000 ± 0.010
57	NGC5846	17.120 ± 0.050	16.100 ± 0.030	12.800 ± 0.010	10.840 ± 0.010	9.980 ± 0.010	9.470 ± 0.010	9.240 ± 0.010
58	SDSSJ150634.25+001255.6		22.701 ± 0.345	18.881 ± 0.077	17.597 ± 0.010	17.030 ± 0.010	16.768 ± 0.012	16.701 ± 0.054
59	PGC3119319	22.363 ± 0.147	21.303 ± 0.089	17.892 ± 0.018	15.857 ± 0.003	15.011 ± 0.003	14.573 ± 0.003	14.220 ± 0.004
60	NGC5841	21.160 ± 0.140	19.070 ± 0.040	15.670 ± 0.010	14.030 ± 0.010	13.260 ± 0.010	12.820 ± 0.010	12.650 ± 0.010
61	PGC1156476		21.833 ± 0.377	19.121 ± 0.063	17.715 ± 0.009	17.069 ± 0.008	16.800 ± 0.010	16.607 ± 0.034
62	PGC1171244	20.682 ± 0.081	20.226 ± 0.054	18.850 ± 0.061	17.661 ± 0.010	17.224 ± 0.010	16.997 ± 0.015	16.930 ± 0.055
63	NGC5846:[MTT2005]226	21.704 ± 0.145	21.268 ± 0.104	19.455 ± 0.128	18.329 ± 0.017	17.842 ± 0.026	17.589 ± 0.022	17.354 ± 0.077

Table 4 – *continued*

Id. No.	Galaxy	FUV (AB mag)	NUV (AB mag)	*u* (AB mag)	*g* (AB mag)	*r* (AB mag)	*i* (AB mag)	*z* (AB mag)
64	NGC5850	15.110 ± 0.050	14.730 ± 0.030	13.030 ± 0.010	11.530 ± 0.010	10.960 ± 0.010	10.560 ± 0.010	10.520 ± 0.010
65	PGC1185172		22.125 ± 0.567	18.628 ± 0.075	17.330 ± 0.009	16.784 ± 0.009	16.526 ± 0.011	16.310 ± 0.028
66	PGC054004	23.673 ± 0.372		17.305 ± 0.037	15.685 ± 0.004	14.985 ± 0.004	14.621 ± 0.004	14.460 ± 0.013
67	NGC5854	19.480 ± 0.060	17.140 ± 0.030	13.950 ± 0.010	12.340 ± 0.010	11.640 ± 0.010	11.230 ± 0.010	11.070 ± 0.010
68	PGC054016			16.938 ± 0.025	15.607 ± 0.003	14.954 ± 0.003	14.613 ± 0.003	14.441 ± 0.009
69	PGC1217593		21.631 ± 0.128	18.972 ± 0.069	17.578 ± 0.009	16.915 ± 0.008	16.578 ± 0.009	16.439 ± 0.045
70	PGC054037			17.274 ± 0.028	15.586 ± 0.004	14.796 ± 0.004	14.419 ± 0.005	14.159 ± 0.013
71	NGC5846:[MTT2005]258	22.202 ± 0.150		20.798 ± 0.565	18.820 ± 0.032	18.363 ± 0.033	18.273 ± 0.046	19.024 ± 0.365
72	NGC5846:[MTT2005]259			20.699 ± 0.413	19.221 ± 0.038	18.579 ± 0.036	18.594 ± 0.059	19.142 ± 0.368
73	PGC054045			18.066 ± 0.073	16.316 ± 0.007	15.630 ± 0.007	15.329 ± 0.018	15.121 ± 0.021
74	SDSSJ150812.35+012959.7			19.487 ± 0.180	17.743 ± 0.014	17.059 ± 0.012	16.705 ± 0.013	16.437 ± 0.042
75	NGC5846:[MTT2005]264			19.821 ± 0.126	18.641 ± 0.018	18.101 ± 0.018	17.789 ± 0.021	17.740 ± 0.087
76	PGC1206166			19.034 ± 0.098	17.634 ± 0.011	16.997 ± 0.010	16.730 ± 0.013	16.765 ± 0.202
77	NGC5846:[MTT2005]268			20.828 ± 0.444	18.919 ± 0.031	18.200 ± 0.116	18.126 ± 0.040	17.774 ± 0.122
78	PGC1209573			17.871 ± 0.038	16.332 ± 0.005	15.682 ± 0.004	15.372 ± 0.005	15.182 ± 0.014
79	PGC1176385	19.943 ± 0.049	19.424 ±0.026	17.661 ± 0.021	16.507 ± 0.004	15.905 ± 0.004	15.607 ± 0.006	15.415 ± 0.014
80	SDSSJ150907.83+004329.7	19.994 ± 0.060	19.637 ±0.044	18.563 ± 0.056	17.429 ± 0.012	16.871 ± 0.012	16.635 ± 0.018	16.688 ± 0.052
81	PGC1210284			17.999 ± 0.050	16.385 ± 0.005	15.702 ± 0.005	15.407 ± 0.006	15.227 ± 0.019
82	NGC5864			14.240 ± 0.010	12.400 ± 0.010	11.630 ± 0.010	11.230 ± 0.010	10.980 ± 0.010
83	NGC5869	19.180 ± 0.060	17.500 ± 0.030	14.420 ± 0.010	12.410 ± 0.010	11.660 ± 0.010	11.150 ± 0.010	10.900 ± 0.010
84	UGC09746		17.150 ± 0.030	15.610 ± 0.010	14.440 ± 0.010	13.860 ± 0.010	13.530 ± 0.010	13.270 ± 0.010
85	UGC09751	19.343 ± 0.044	18.533 ± 0.025	17.492 ± 0.041	16.108 ± 0.006	15.577 ± 0.006	15.326 ± 0.009	15.264 ± 0.021
86	PGC1202458			18.625 ± 0.083	17.018 ± 0.014	16.360 ± 0.013	16.046 ± 0.013	16.047 ± 0.099
87	SDSSJ151121.37+013639.5			18.987 ± 0.151	17.152 ± 0.012	16.488 ± 0.018	16.288 ± 0.019	16.177 ± 0.044
88	UCG09760	17.380 ± 0.050	17.020 ± 0.030	16.200 ± 0.010	15.030 ± 0.010	14.680 ± 0.010	14.530 ± 0.010	14.450 ± 0.010
89	PGC1199418			17.940 ± 0.030	16.662 ± 0.006	16.134 ± 0.005	15.864 ± 0.006	15.704 ± 0.014
90	PGC1215336		20.601 ± 0.066	18.124 ± 0.049	16.646 ± 0.006	16.007 ± 0.005	15.683 ± 0.006	15.480 ± 0.022

(right-hand panels) colour composite images of all 90 galaxy members. The HYPERLEDA optical morphological classification is in good agreement with that suggested by UV images.

Here, we present the galaxies of the group for which UV images suggest a different morphological classification.

ID 15: NGC 5811 is a blue UV galaxy with a bar, visible both in optical and UV, representing the main body of the galaxy. It is a late-type galaxy, SBm, rather than dE.

ID 20: SDSSJ150100.85+010049.8, we adopted the HYPERLEDA classification.

ID 28: UGC09661 shows a blue bar in UV, the SBd classification seems more appropriate than Sdm.

ID 35: PGC087108, shows two distinct bright sources in a common blue envelope in the UV image. It is classified as Irregular; the classification seems correct.

ID 47: PGC1190358 morphology is quite irregular in the UV image. It does not appear a dE as in Mahdavi et al. (2005).

ID 53: PGC 1218738 seems to have a blue inner bar in the UV image although it is classified Sm.

ID 55: PGC1215798, classified Scd, shows peculiar tidal tails, that we consider as possible interaction signatures.

ID 58: SDSSJ150634.25+001255.6. We consider this galaxy a dE (T = −5 ± 5) as in HYPERLEDA.

ID 60: NGC 5841 is an S0-a, incipient arms are visible in the SDSS image. The UV composite image shows that the colour is consistent with an old stellar population.

ID 64: NGC5850 is a barred Spiral with a ring and irregular spiral arms, likely signatures of interaction. The irregular arms are markedly extended in the UV image much further out than the optical size. We suggest a classification of SB(r)b as in RC3.

ID 65: PGC1185172 is classified S? (T = 10 ± 5). We adopted the dE classification of Mahdavi et al. (2005).

ID 67: NGC 5854 is classified S0-a in HYPERLEDA and S0 in Mahdavi et al. (2005). The UV image suggests the presence of incipient arms, more consistent with the HYPERLEDA classification.

ID 70: PGC054037 is classified S? in HYPERLEDA (T = 1 ± −5) and S0a in Mahdavi et al. (2005). We adopt this latter classification.

ID 80: PGC4005496 appears quite blue in UV composite image and with an irregular shape. Rather than a E/dE classification we suggest Im.

ID 88: UGC09760, seen edge-on, is classified Scd/Sd. The yellow spot on the blue galaxy disc of the UV image is a star. The galaxy appears really bulge-less, so we adopted the morphological classification given in RC3, i.e. Sd.

ID 90: PGC1215336 is classified S? (T = 10 ± 5). We classified it as dE from the SDSS image.

4.2 The UV–optical CMD

Fig. 6 shows the UV–optical CMDs of the members of NGC 5846. In the M_r versus NUV−r CMD (bottom panel), there are 69 galaxies and 75 per cent are dwarfs, as previously defined. The red sequence, where passively evolving galaxies are located, is well defined and populated by both Ellipticals and S0s. ETGs represent 82 per cent (56/69) of the total galaxy population and 79 per cent (44/56) of them are dwarfs. The 33 per cent (14/44) of galaxies fainter than $M_r = -18$ are ETGs lying in the ‘green valley’, i.e. with $2 \leq$ NUV−r ≤ 4, some of them very near to the blue sequence. This behaviour agrees with the findings of Mazzei, Marino & Rampazzo (2014). These authors, studying the evolution of ETGs in two groups of the Leo cloud, USCG U376, and LGG 225, found that rejuvenation episodes are more frequent in fainter ETGs (see their fig. 5).

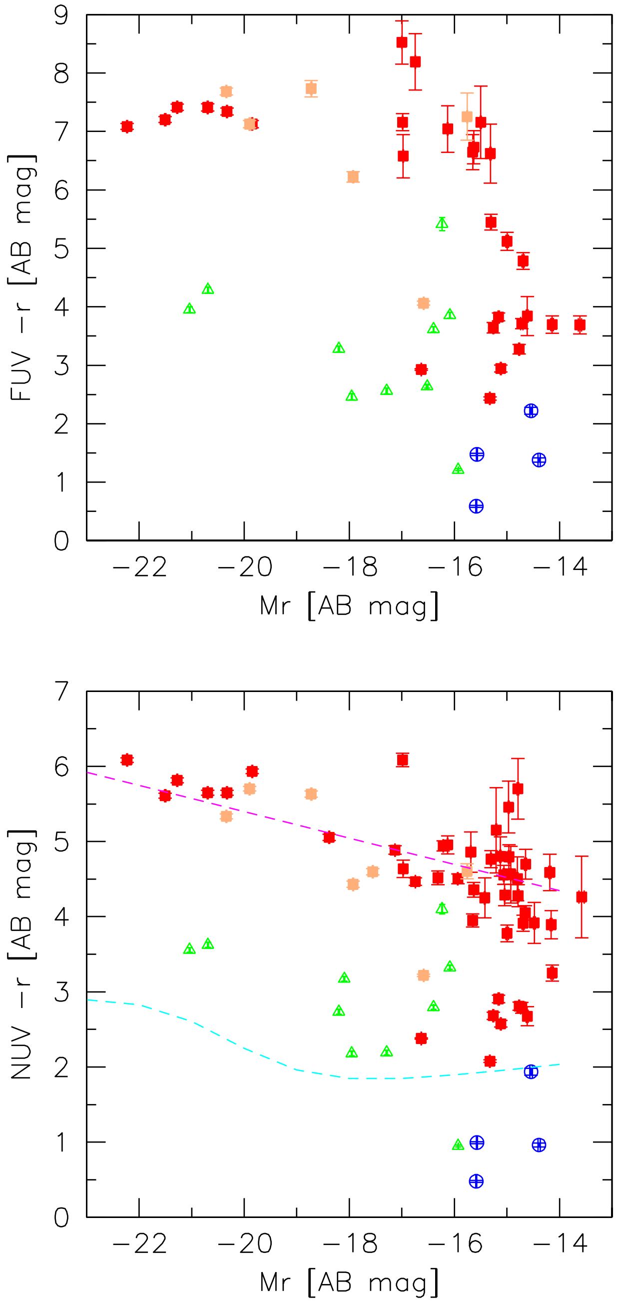

Figure 6. UV–optical CMDs of NGC 5846. Top: M_r versus FUV$-r$. Bottom: M_r versus NUV$-r$. In the M_r versus NUV$-r$ CMD, we overplot the Wyder et al. (2007) fits to the red and blue galaxy sequences. Green triangles mark Spirals, Ellipticals and S0s are indicated with red and orange squares, respectively, and blue circles show Irregulars. The magnitudes were corrected by Galactic extinction (Burstein & Heiles 1982).

Fig. 7 shows the absolute *B* magnitude, M_B, versus NUV$-i$ of the group members (top panel). In the bottom panel of Fig. 7, the cumulative distribution of NUV$-i$ for normal and dwarf members of the group is shown. The distribution gives the fraction of normal and dwarf galaxies in the group that have a colour greater (redder) than a given value of NUV$-i$. For example, ∼90 and 20 per cent of normal and dwarf galaxies, respectively, have NUV$-i > 5$. According to the Kolmogorov–Smirnov test, the null hypothesis that two distributions are drawn from the same parent distribution can be rejected at a confidence level >99 per cent. We consider the hypothesis that giant ETGs members may either have formed through

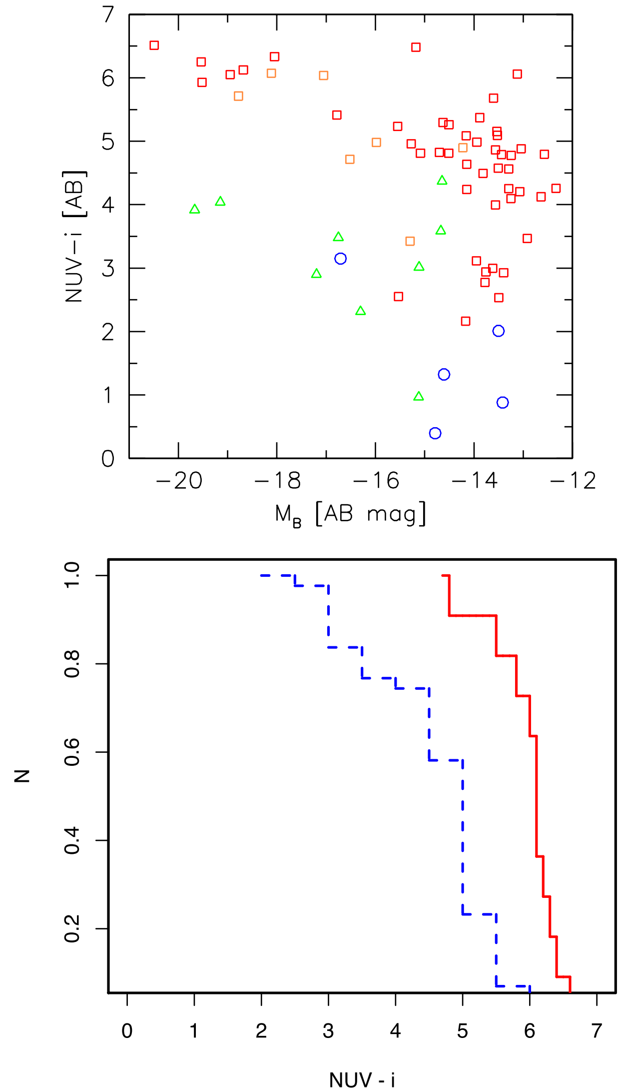

Figure 7. Top: the M_B versus NUV$-i$ CMD of the group members. Symbols are as in Fig. 6. Bottom: cumulative distributions of NUV−i of dwarf (blue dashed line) and normal (red continuous line) ETGs in our group; according to the Kolmogorov–Smirnov test the null hypothesis, that the two distributions are drawn from a same parent distribution, can be rejected at a confidence level > 99 per cent.

or have experienced a significant number of accretions of dwarfs galaxies during the evolution of the group. In this hypothesis, the colour distributions of the two samples should have similar characteristics.

This should be particularly true if the accretions have been ‘dry’, i.e. the accretion has been ‘sterile’ not igniting star formation episodes.

The statistically significant difference of the NUV$-i$ of dwarfs and giant ETGs rules out the above formation scenario and a ‘dry’ accretion scenario. Instead, we suggest that in the star formation history of both dwarfs and normal ETGs, gas dissipation cannot be neglected. We further explore this hypothesis in the following section.

4.3 The colour–colour FUV$-$NUV versus NUV$-r$ diagram

The slope of the UV spectrum is related to the temperature of the stars emitting in the UV and their relative contribution to the total

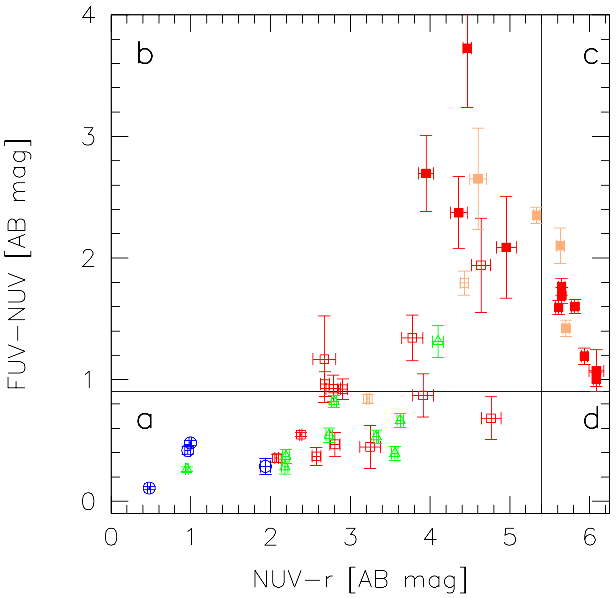

Figure 8. The FUV−NUV versus NUV−r colour–colour diagram of the NGC 5846 group members. Symbols are as in the previous figures. The magnitudes were corrected by Galactic extinction following Burstein & Heiles (1982). Solid lines correspond to FUV−NUV = 0.9, i.e UV rising slope, and NUV−r = 5.4, i.e. a galaxy devoid of young massive stars. These conditions, following the UV classification scheme by Yi et al. (2011), separate passive evolving ETGs (region b) from star-forming galaxies (region a), see text). Filled symbols are for galaxies with FUV−$r \geq$ 6.6 mag.

flux. The value FUV−NUV = 0.9 indicates a flat UV spectrum in the λ − versus F_λ domain, whereas a negative FUV−NUV corresponds to a bluer population. Yi et al. (2011) established a colour criterion to classify ETGs according to their UV spectral morphology based on three colour. Passively evolving ETGs would have NUV−$r \geq$ 5.4, and FUV−$r \geq$ 6.6. These values indicate the average value of the red sequence in Fig. 6. ETGs showing UV upturn with no residual star formation have to obey a further condition, FUV−NUV < 0.9. Fig. 8 shows the position of NGC 5846 group members in the colour–colour UV–optical diagram emphasizing their morphological classification. The same fraction of dwarf ETGs which stays in the 'green valley' of Fig. 6, i.e. 33 per cent, lies in the region where residual star formation is expected (region a in Fig. 8), in good agreement with findings of Mazzei et al. (2014). All the ETGs brighter than −18 in the r band (Fig. 6, top panel) show red FUV−r colours and FUV−NUV > 0.9 and lie in the regions (b) and (c) of Fig. 8. The brightest members of this group, i.e. NGC 5846 and NGC 5813, lie in the right-upper region of this colour–colour diagram, i.e. region (c), where passively evolving ETGs would stay according the Yi et al. (2011) criterion. No galaxies are found in region (d) of Fig. 8, where ETGs with UV upturn and no residual star formation would lie.

5 COMPARISON WITH OTHER GROUPS AND THE VIRGO CLUSTER

Fig. 9 shows the cumulative distribution of the FUV−NUV colours of NGC5846, and of three groups already analysed in the Leo cloud (Paper I and II). This figure points out that the fraction of red UV colours, i.e. FUV−NUV > 0.9, increases with increasing number of ETGs. By comparing Fig. 6 (bottom) with figs 10 and 11 in Paper II we note that the number of galaxies with red NUV−r colours, i.e.

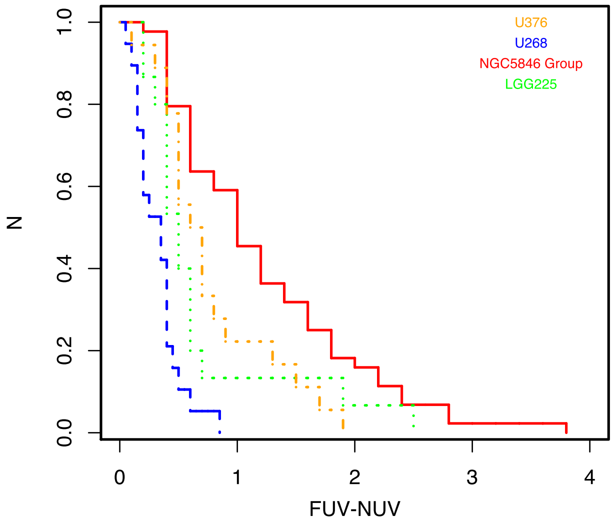

Figure 9. Cumulative distribution of FUV−NUV colours of galaxies in NGC5846 group (solid line), and in three groups previously studied, i.e, U268 (dashed line), U376 (dot–dashed line), and LGG225 (dotted line).

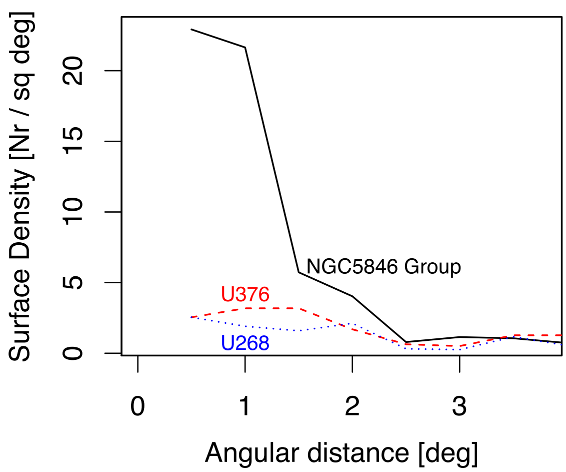

Figure 10. Surface member density as a function of the radial distance from the centre of mass defined by the dynamical analysis developed in Section 2.4. For comparison, the surface density distributions of the two groups U268 (dotted line) and U376 (dashed line) are shown.

along the red sequence, all ETGs, increases with the groups are more massive and composed by more galaxies.

Fig. 10 compares the density distribution versus angular distance from the dynamical centre of NGC 5486 (solid line) with the density distribution of the groups previously studied, i.e, USGC U376 (dashed line) and USGC U268 (dotted line). These latter groups are located in the Leo cloud. The dynamical analysis by Marino et al. (2014) suggests that USGC U268 is in a pre-virial collapse phase while U376 seems in a more evolved phase towards virialization. Notice that our distribution is different from that shown in Mahdavi et al. (2005, their fig. 7) because we use the centre of mass of the group (Table 2) as centre of the density distribution. We obtain the same distribution as Mahdavi et al. (2005) if we select NGC 5486 as centre of the group.

Fig. 11 shows the UV luminosity function (LF hereafter; top panel FUV and bottom panel NUV) of NGC 5846 group. For comparison we plot, on the same scale, the UV LFs of the Virgo cluster (dotted line) as in fig. 8 of Boselli & Gavazzi (2014). These authors noted

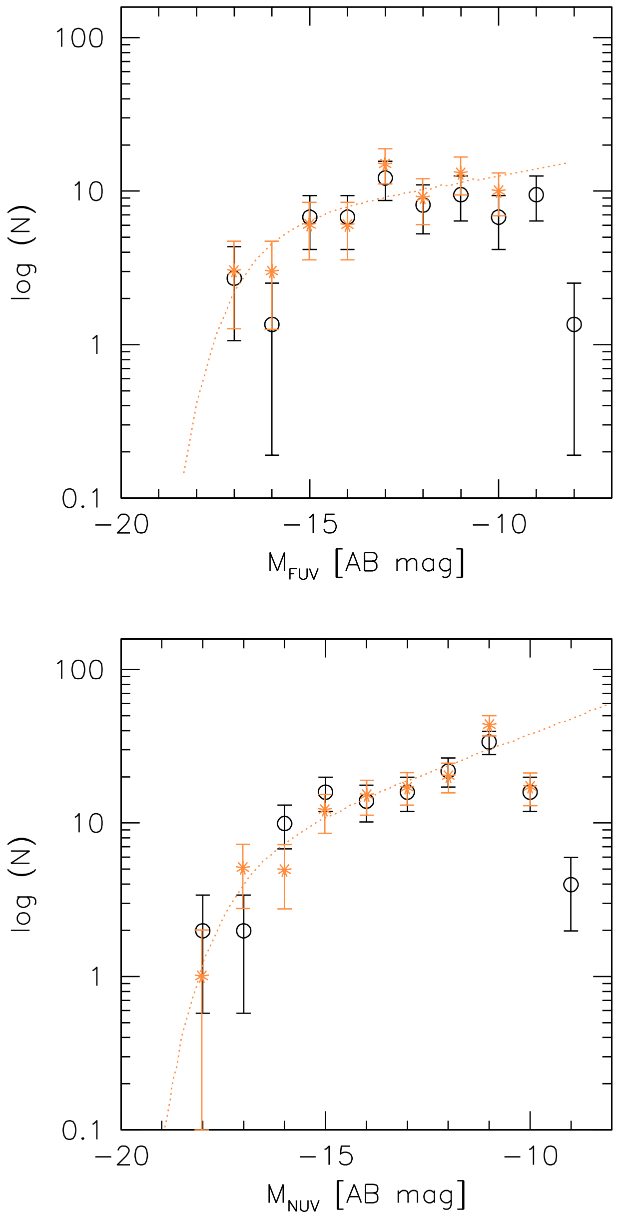

Figure 11. The FUV and NUV LFs of NGC 5846 group (open circles) compared to those of the Virgo cluster (asterisks; dotted line shows the fit limited to −13 mag by Boselli & Gavazzi (2014). LFs have been normalized to include the same galaxy number as Virgo, i.e. 135 in NUV and 65 in FUV as in Boselli & Gavazzi (2014).

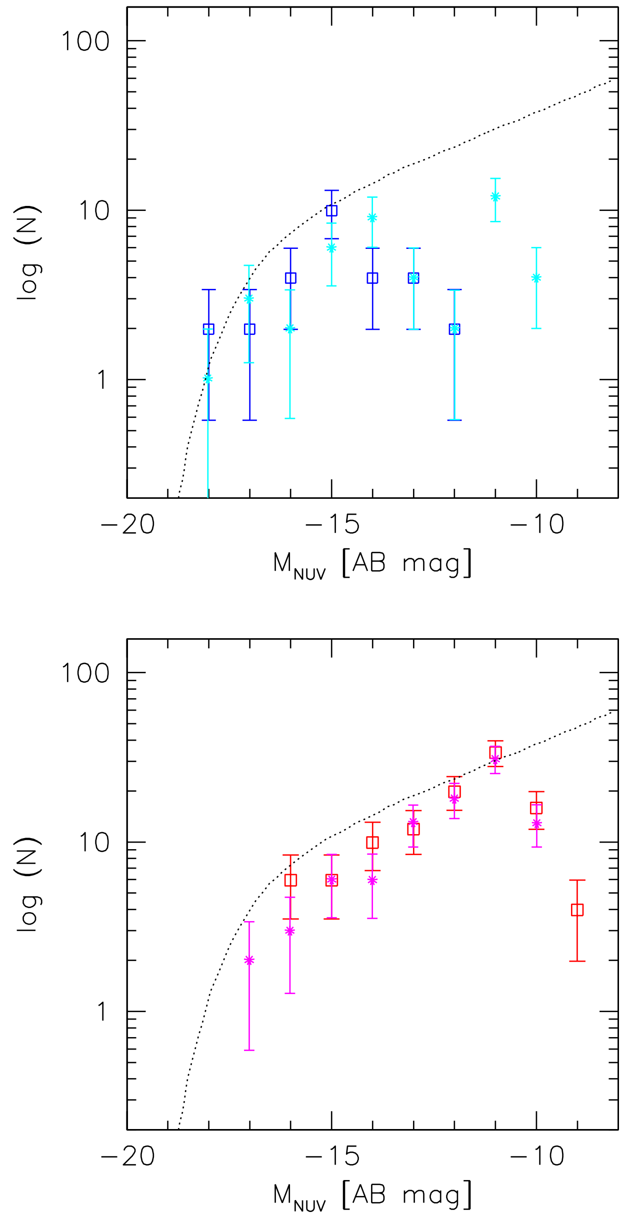

Figure 12. The NUV LFs of NGC 5846 group splitted in late-type galaxies (top), and ETGs (bottom), compared to those of the Virgo cluster (asterisks and dotted line as in Fig. 11) from Boselli & Gavazzi (2014, their fig. 14).

that the NUV and FUV LFs of Virgo and the field are similar. We find that FUV and NUV LFs of NGC 5846 group are quite similar to those of the Virgo cluster. In particular, as shown in Fig. 12, also the LFs of late-type galaxies and ETGs in both groups are quite indistinguishable from those of this cluster.

Fig. 13 shows that the shape of the FUV and NUV LFs in less dense groups (see Fig. 10) is dominated by late-type galaxies. In the brightest magnitude bins, late-type galaxies are more numerous in these groups than in denser groups like NGC 5846 and Virgo.

6 SUMMARY AND CONCLUSIONS

This paper is the third of a series dedicated to the study of nearby groups with a different morphological mix of galaxy populations and sampling different dynamical phases.

We have obtained FUV and NUV *GALEX* and SDSS – *u*, *g*, *r*, *i*, *z* AB magnitudes of 90 spectroscopically confirmed members of NGC 5846, the third most massive nearby association after Virgo and Fornax nearby clusters. The backbone of the group comes from the catalogue of Ramella et al. (2002) that we enriched of members applying kinematical and dynamical selection criteria to galaxies with known optical redshift (see also Paper I and II).

The group membership as well as the characteristics of the group have been already investigated with a different method by Mahdavi et al. (2005) and Eigenthaler & Zeilinger (2010). Our selection of 90 members includes all the spectroscopically confirmed members of Mahdavi et al. (2005) and Eigenthaler & Zeilinger (2010) plus two ETGs in HYPERLEDA meeting our criteria.

The kinematical and dynamical analysis of the group indicates that it is in an evolved phase according to Mahdavi et al. (2005) analysis. The main novelty of this study is the UV analysis. Our

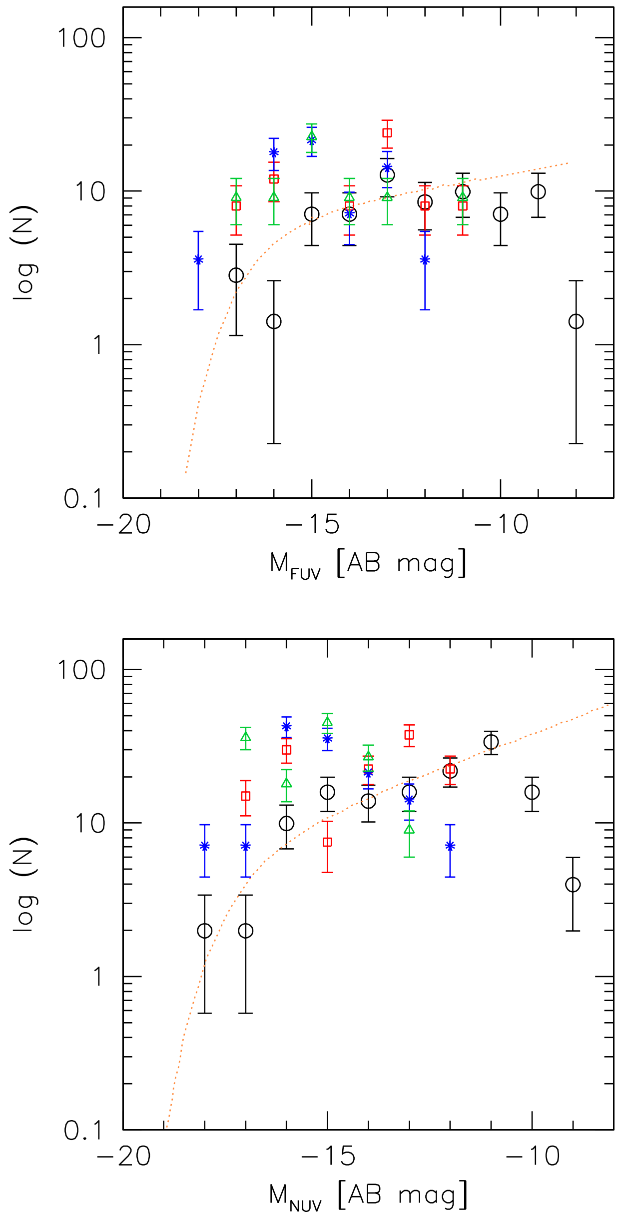

Figure 13. The FUV and NUV LFs of NGC 5846 group (circles) compared to those of the Virgo cluster (dotted line; Boselli & Gavazzi 2014), U376 (red squares), U268 (blue asterisks), and LGG225 (green triangles). LFs have been normalized as in Fig. 11.

analysis of the UV data shows that a large fraction of dEs (33 per cent, Section 4.3) does not reside in the red or in the blue sequence of the group CMD but it lies in the 'green valley', where 'rejuvenation' episodes of dEs occur with higher frequency (Mazzei et al. 2014). We find that only 5 per cent of the total ETG population of the group lies in the region of passively evolving ETGs (Section 4.3, region c, Fig. 8) whereas dEs are found in the locus of star forming galaxies (region a, Fig. 8). Moreover, by analysing the cumulative NUV$-i$ colour distributions of dEs and normal ETGs in the group, the hypothesis that the two distributions are drawn from the same parent distribution can be rejected at a confidence level of >99 per cent. We concluded that the UV–optical colours of normal ETGs in the group cannot be accounted by dry mergers of the dE population: gas dissipation, i.e. star formation, cannot be neglected in the evolution of the group members.

Boselli & Gavazzi (2014) found that Virgo galaxies are quenched by ram pressure and suggest that the quenching of the star formation activity in dwarf systems and the formation of the faint end of the red sequence is a very recent phenomenon. Although the UV LFs of both Virgo and NGC 5846 are very similar, only a small fraction of galaxies in NGC 5846 is passively evolving. Our UV–optical analysis suggests that star formation events are still occurring in this group, in particular in its dwarf ETG population, tracing a picture of a still active phase notwithstanding its large number of ETGs and its likely virialized configuration (Table 2).

Mazzei et al. (2014), investigating the evolution of the brightest ETGs in the U376 and LGG 225 groups, found that residual star formation, i.e. 'rejuvenation', is luminosity dependent so that bursts of star formation can occur still today in dEs, as found in this group.

In a forthcoming paper (Mazzei et al., in preparation), we will investigate further the evolution of the brightest ETG members and some dwarfs of this group using a smooth particle Hydrodynamic code with chemo-photometric implementation. We will also expand the study to other selected groups for which we have UV and optical images.

ACKNOWLEDGEMENTS

We acknowledge the usage of the HYPERLEDA and NED data bases. Paola Mazzei and Roberto Rampazzo acknowledge support from INAF through grant PRIN-2014-14 'Star formation and evolution in galactic nuclei'.

Facilities: *GALEX*, Sloan.

REFERENCES

Adelman-McCarthy J. K., Agüeros M. A., Allam S. S., Allende Prieto C., Anderson K. S. J., Anderson S. F., Annis J., Bahcall N. A., 2008, ApJS, 175, 297
Balogh M. L., Baldry I. K., Nichol R., Miller C., Bower R., Glazebrook K., 2004, ApJ, 615, L101
Barnes J. E., 2002, MNRAS, 333, 481
Bianchi L., 2009, Ap&SS, 320, 11
Bianchi L., 2014, Ap&SS, 354, 103
Bianchi L., Efremova B., Herald J., Girardi L., Zabot A., Marigo P., Martin C., 2011, MNRAS, 411, 2770
Boselli A., Gavazzi G., 2014, A&AR, 22, 74
Burstein D., Heiles C., 1982, AJ, 87, 1165
Cardelli J. A., Clayton G. C., Mathis J. S., 1989, ApJ, 345, 245
Davis M., Geller M. J., 1976, ApJ, 208, 13
Di Matteo T., Springel V., Hernquist L., 2005, in Merloni A., Nayakshin S., Sunyaev R. A., eds, Growing Black Holes: Accretion in a Cosmological Context. Springer-Verlag, Berlin, p. 340
Dressler A., 1980, ApJ, 236, 351
Dressler A., Shectman S. A., 1988, AJ, 95, 985 (DS)
Efron B., 1982, The Jackknife, the Bootstrap and Other Resampling Plans. Soc. Ind. Appl. Math., Philadelphia
Eigenthaler P., Zeilinger W. W., 2010, A&A, 511, A12
Eke V. R., Baugh C. M., Cole S., Frenk C. S., Norberg P., Peacock J. A., 2004, MNRAS, 348, 866
Ferguson H. C., Sandage A., 1990, AJ, 100, 1
Ferguson H. C., Sandage A., 1991, AJ, 101, 765
Firth P., Evstigneeva E. A., Jones J. B., Drinkwater M. J., Phillipps S., Gregg M. D., 2006, MNRAS, 372, 1856
Giuricin G., Marinoni C., Ceriani L., Pisani A., 2000, ApJ, 543, 178
Gómez P. L. et al., 2003, ApJ, 584, 210
Goto T., Yamauchi C., Fujita Y., Okamura S., Sekiguchi M., Smail I., Bernardi M., Gomez P. L., 2003, MNRAS, 346, 601
Haynes M. P., Giovanelli R., 1991, AJ, 102, 841
Hou A. et al., 2012, MNRAS, 421, 3594

Jedrzejewski R. I., 1987, MNRAS, 226, 747
Kawata D., Mulchaey J. S., 2008, ApJ, 672, L103
Lewis I. et al., 2002, MNRAS, 334, 673
Machacek M. E., Jerius D., Kraft R., Forman W. R., Jones C., Randall S., Giacintucci S., Sun M., 2011, ApJ, 743, 15
Mahdavi A., Trentham N., Tully R. B., 2005, AJ, 130, 1502
Makarov D., Prugniel P., Terekhova N., Courtois H., Vauglin I., 2014, A&A, 570, A13
Mamon G. A., 1992, ApJ, 401, L3
Marino A., Bianchi L., Rampazzo R., Buson L. M., Bettoni D., 2010, A&A, 511, A29 (Paper I)
Marino A. et al., 2013, MNRAS, 428, 476 (Paper II)
Marino A., Bianchi L., Mazzei P., Rampazzo R., Galletta G., 2014, Adv. Space Res., 53, 920
Martin D. C. et al., 2005, ApJ, 619, L1
Mazzei P., Marino A., Rampazzo R., 2014, ApJ, 782, 53
Moore B., Katz N., Lake G., Dressler A., Oemler A., 1996, Nature, 379, 613
Morrissey P., Conrow T., Barlow T. A., Small T., Seibert M., Wyder T. K., Budavári, 2007, ApJS, 173, 682
Mulchaey J. S., Davis D. S., Mushotzky R. F., Burstein D., 2003, ApJS, 145, 39
Nolthenius R., 1993, ApJS, 85, 1
Perea J., del Olmo A., Moles M., 1990, Ap&SS, 170, 347
Poggianti B. M. et al., 2006, ApJ, 642, 188
Ramella M., Geller M. J., Pisani A., da Costa L. N., 2002, AJ, 123, 2976
Rampazzo R., Panuzzo P., Vega O., Marino A., Bressan A., Clemens M. S., 2013, MNRAS, 432, 374
Randall S. W. et al., 2011, ApJ, 726, 86
Schawinski K. et al., 2007, ApJS, 173, 512
Silverman B. W., 1986, Monographs on Statistics and Applied Probability. Chapman and Hall, London
Tago E., Einasto J., Saar E., Tempel E., Einasto M., Vennik J., Müller V., 2008, A&A, 479, 927
Tammann G. A., 1994, in Meylan G., Prugniel P., eds, ESO Conf. Workshop Proc. Vol. 49, Dwarf Galaxies in the Past. p. 3
Toomre A., Toomre J., 1972, ApJ, 178, 623
Trinchieri G., Goudfrooij P., 2002, A&A, 386, 472
Tully R. B., 1987, ApJ, 321, 280
Tully R. B., 1988, Nearby galaxies catalog. Cambridge Univ. Press, Cambridge
Werner N., Zhuravleva I., Churazov E., Simionescu A., Allen S. W., Forman W., Jones C., Kaastra J. S., 2009, MNRAS, 398, 23
Werner N. et al., 2014, MNRAS, 439, 2291
Wyder T. K. et al., 2007, ApJS, 173, 293
Yi S. K., Lee J., Sheen Y.-K., Jeong H., Suh H., Oh K., 2011, ApJS, 195, 22

APPENDIX A: UV AND OPTICAL IMAGES OF GALAXIES IN NGC 5846

Fig. A1 shows the UV and optical colour composite images of the members of NGC 5846. The size of each image is 5 × 5 arcmin. 1 arcmin (bar shown) corresponds to ≈7 kpc at the distance of the group.

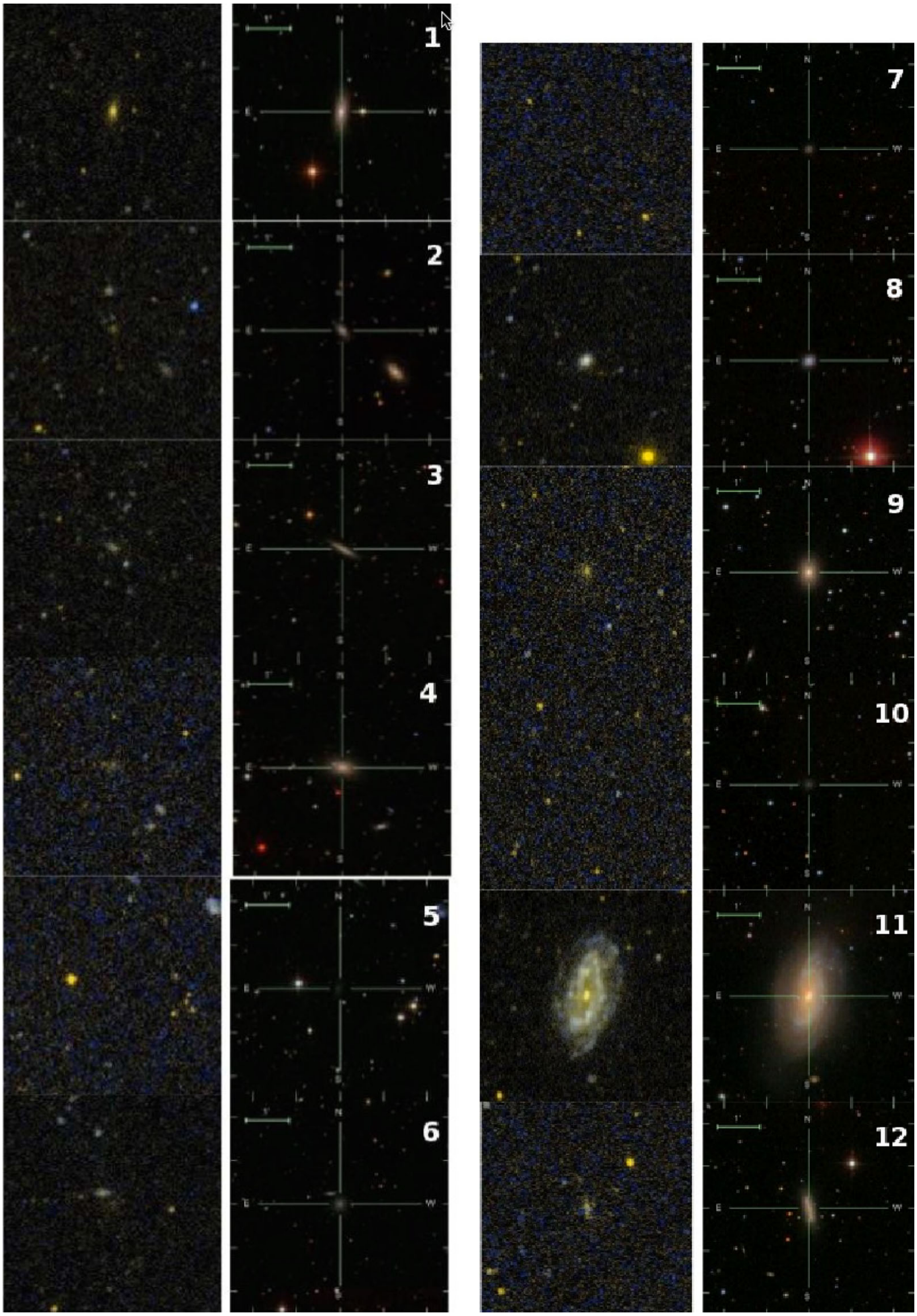

Figure A1. UV (FUV, blue, NUV, yellow, left) and optical (SDSS: *g*, *r*, *i* are blue, green and red, respectively, right) images of members of NGC 5846.

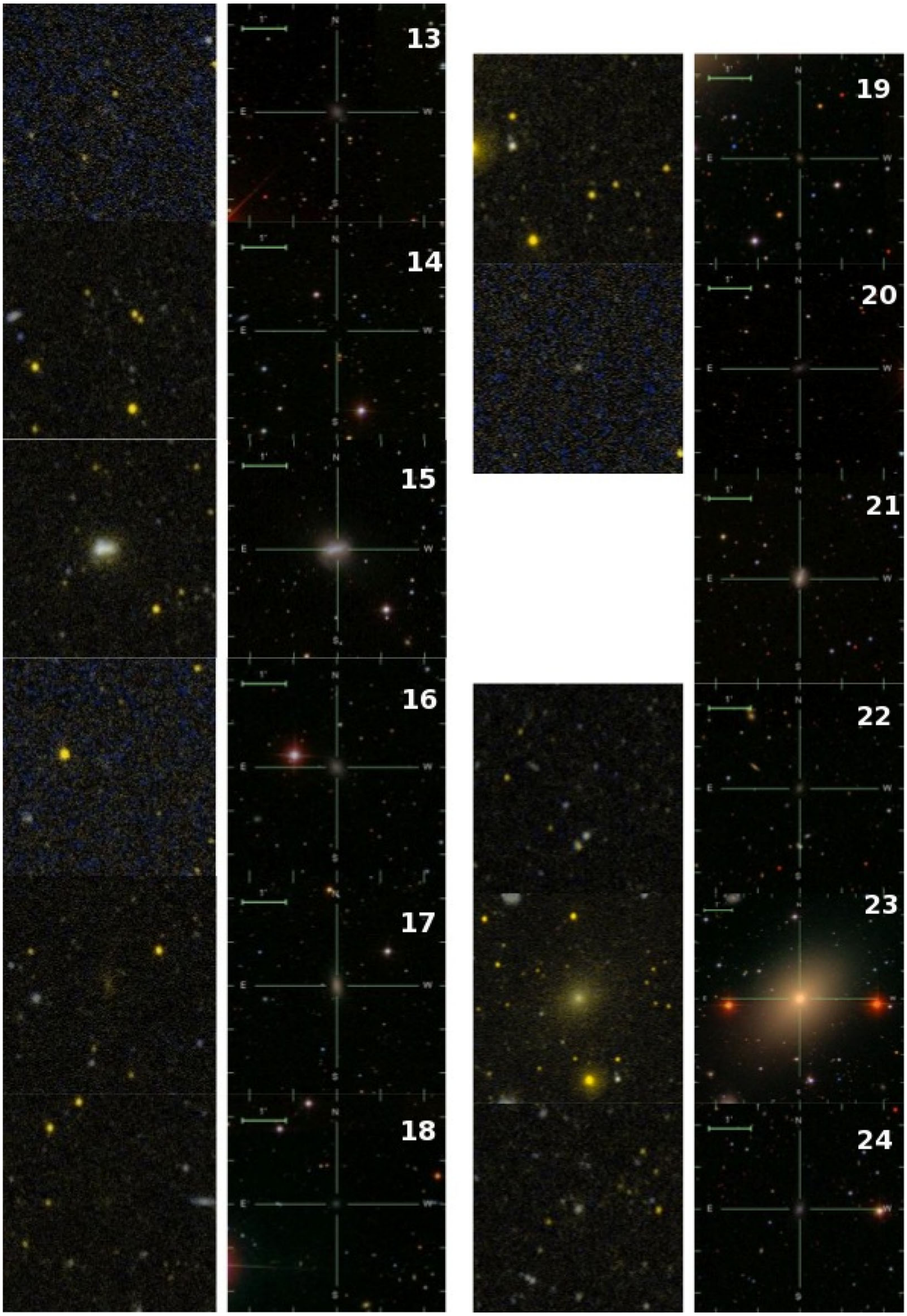

Figure A1 – *continued*

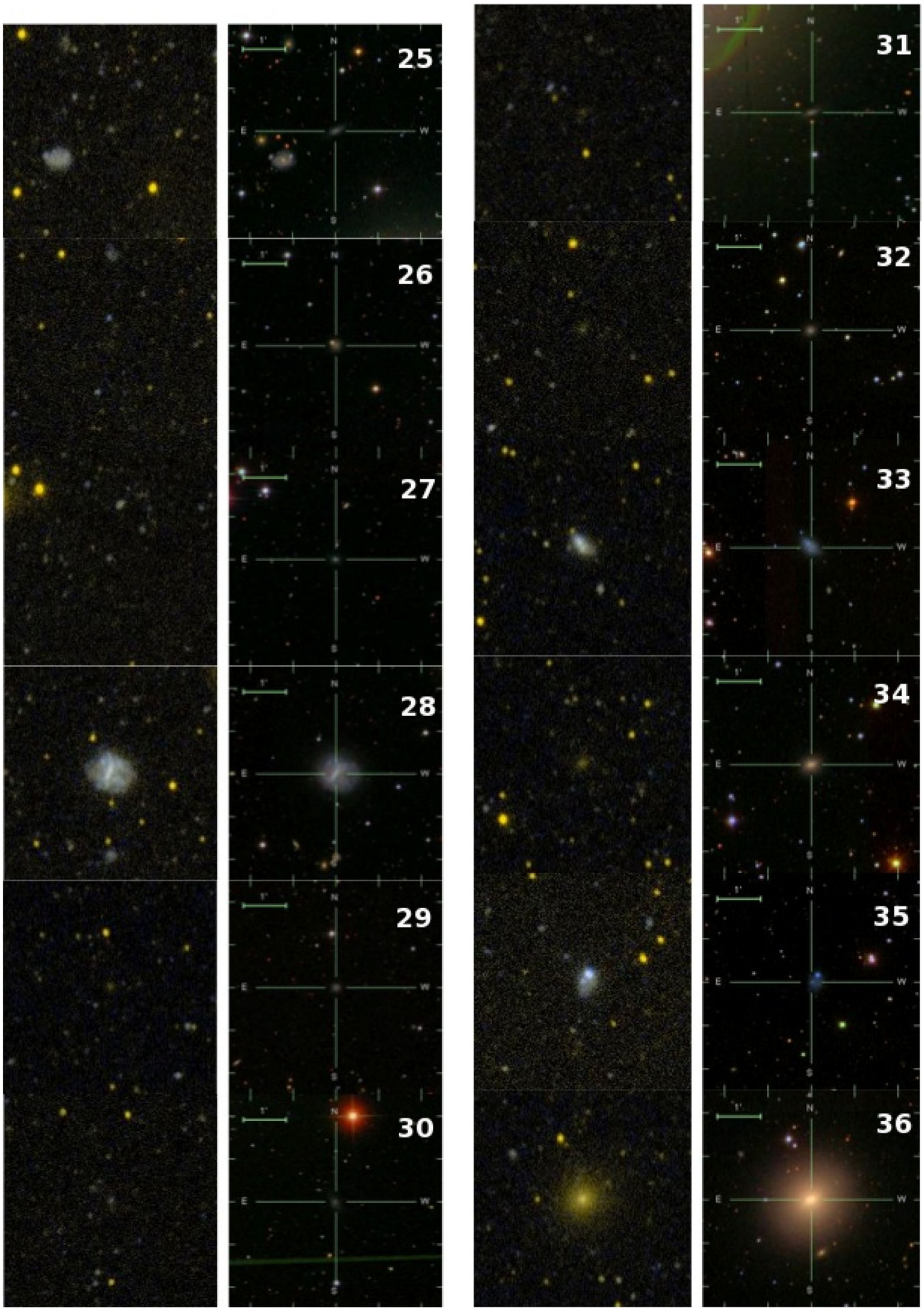

Figure A1 – *continued*

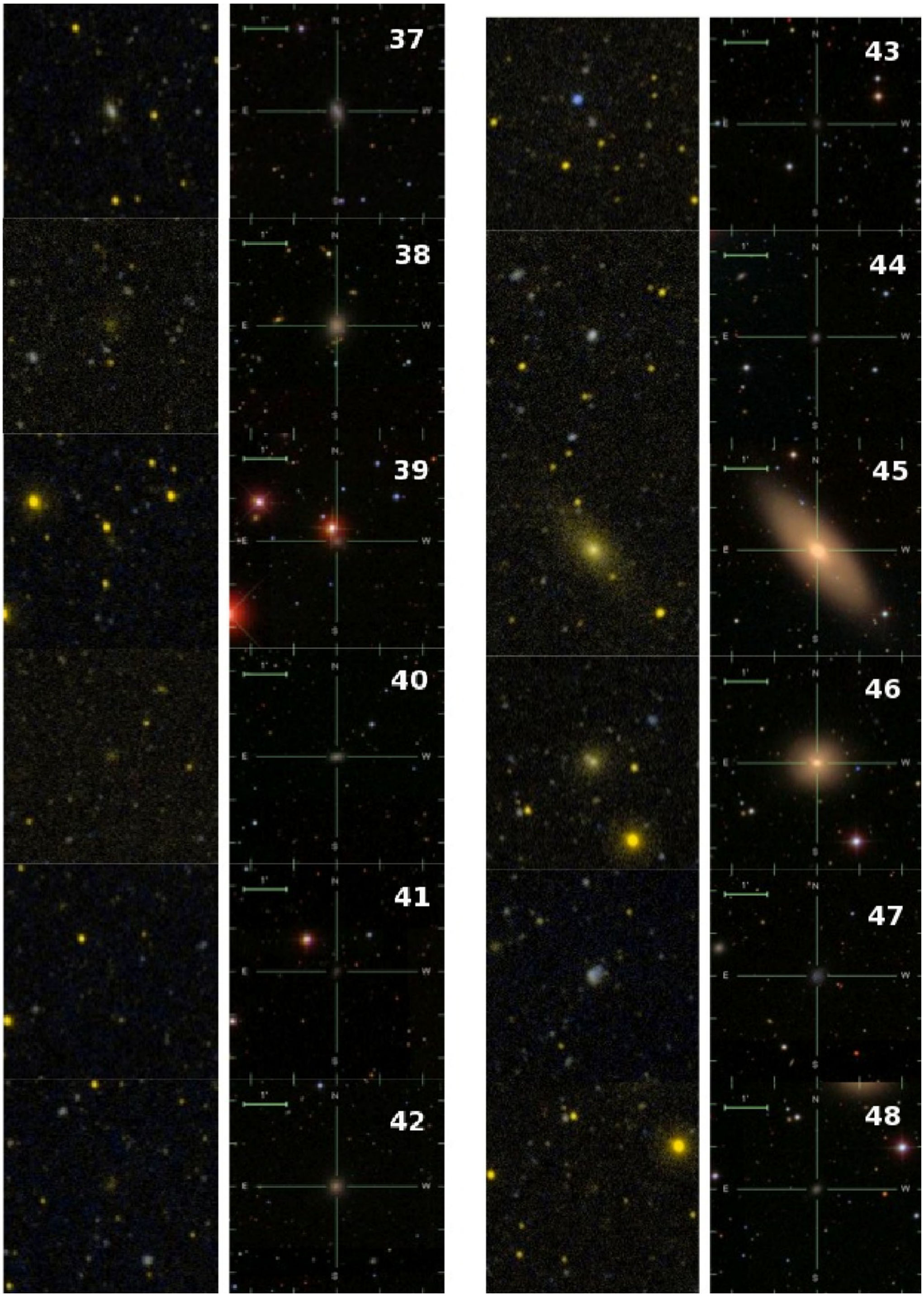

Figure A1 – *continued*

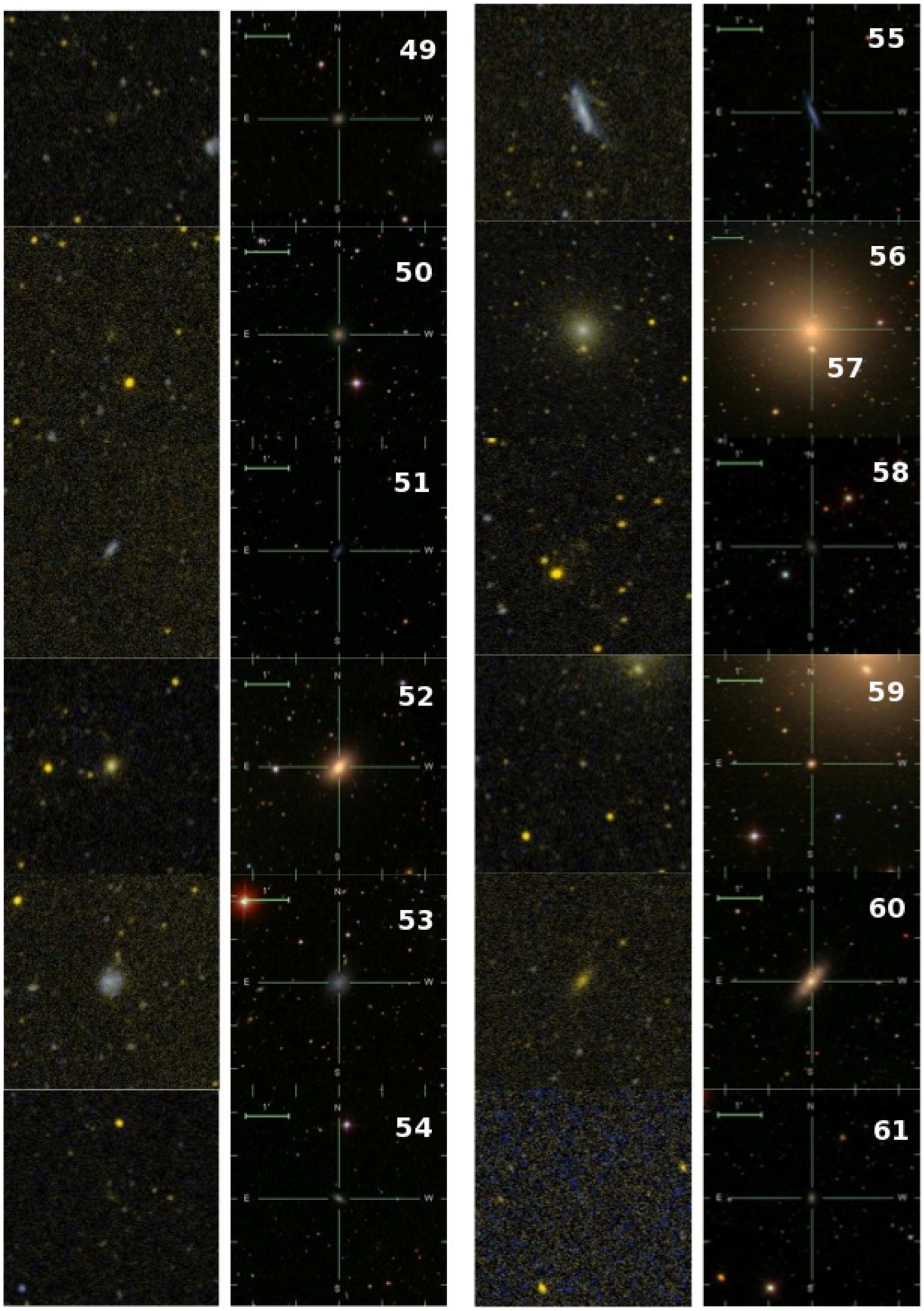

Figure A1 – *continued*

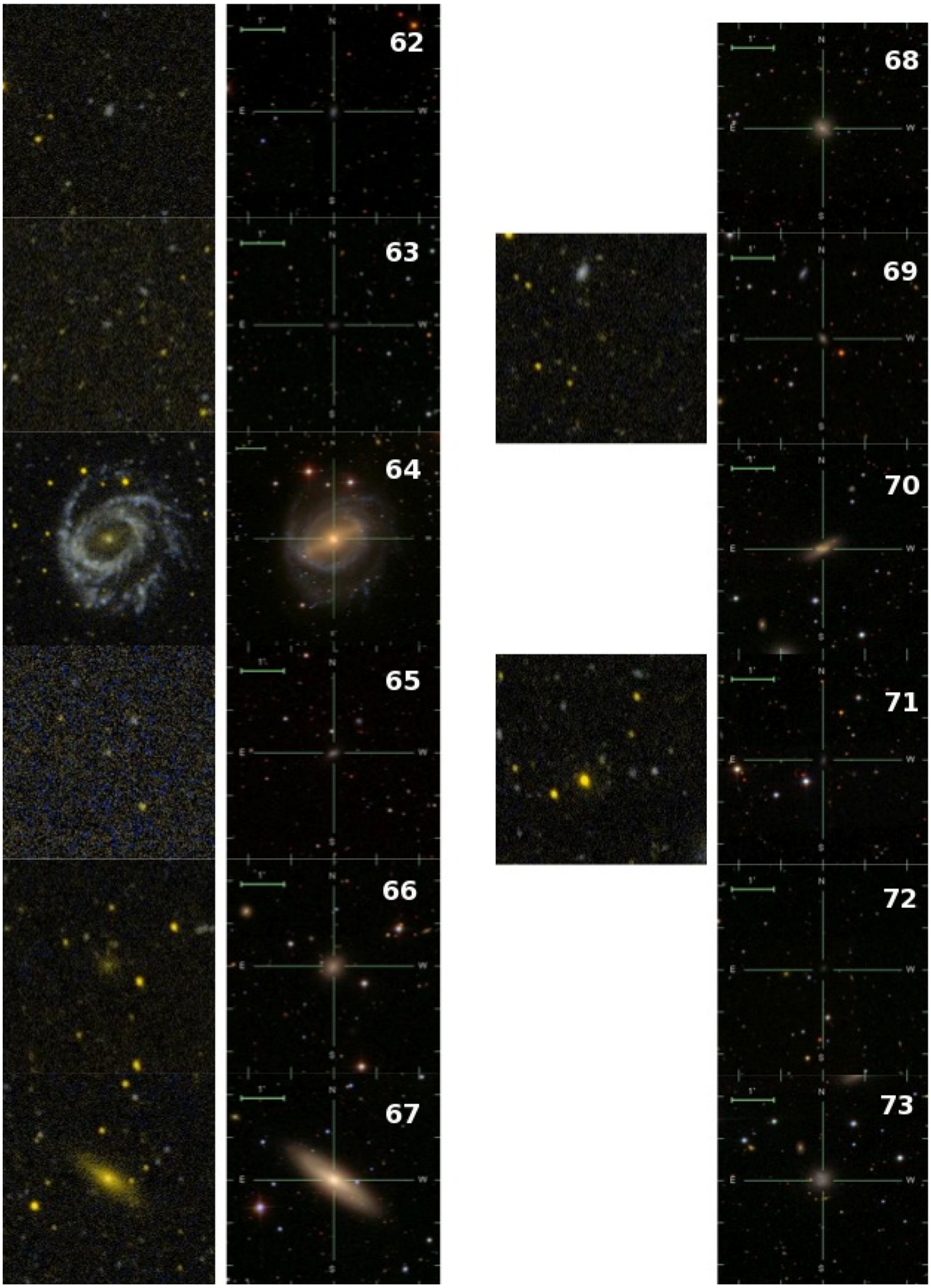

Figure A1 – *continued*

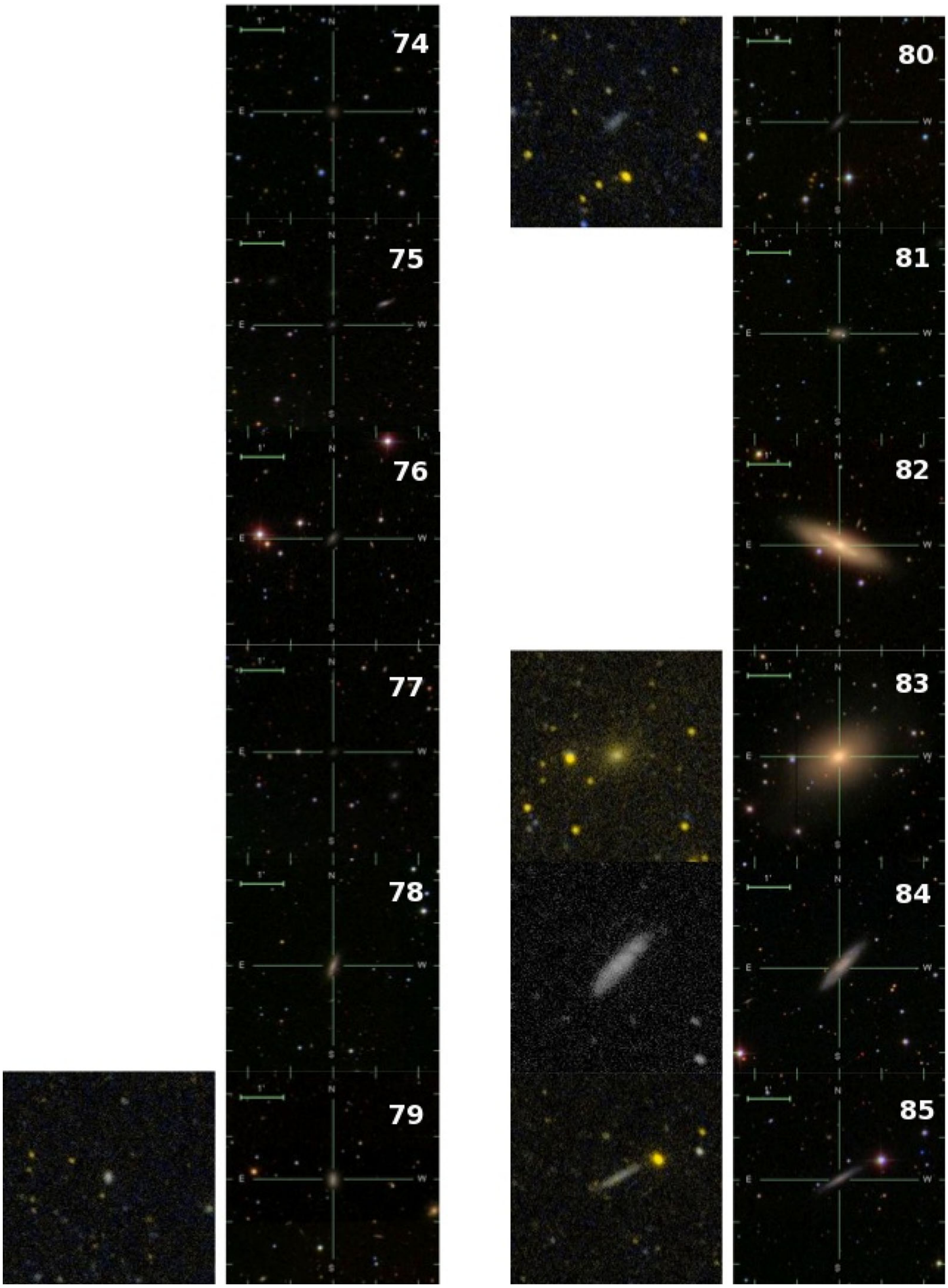

Figure A1 – *continued*

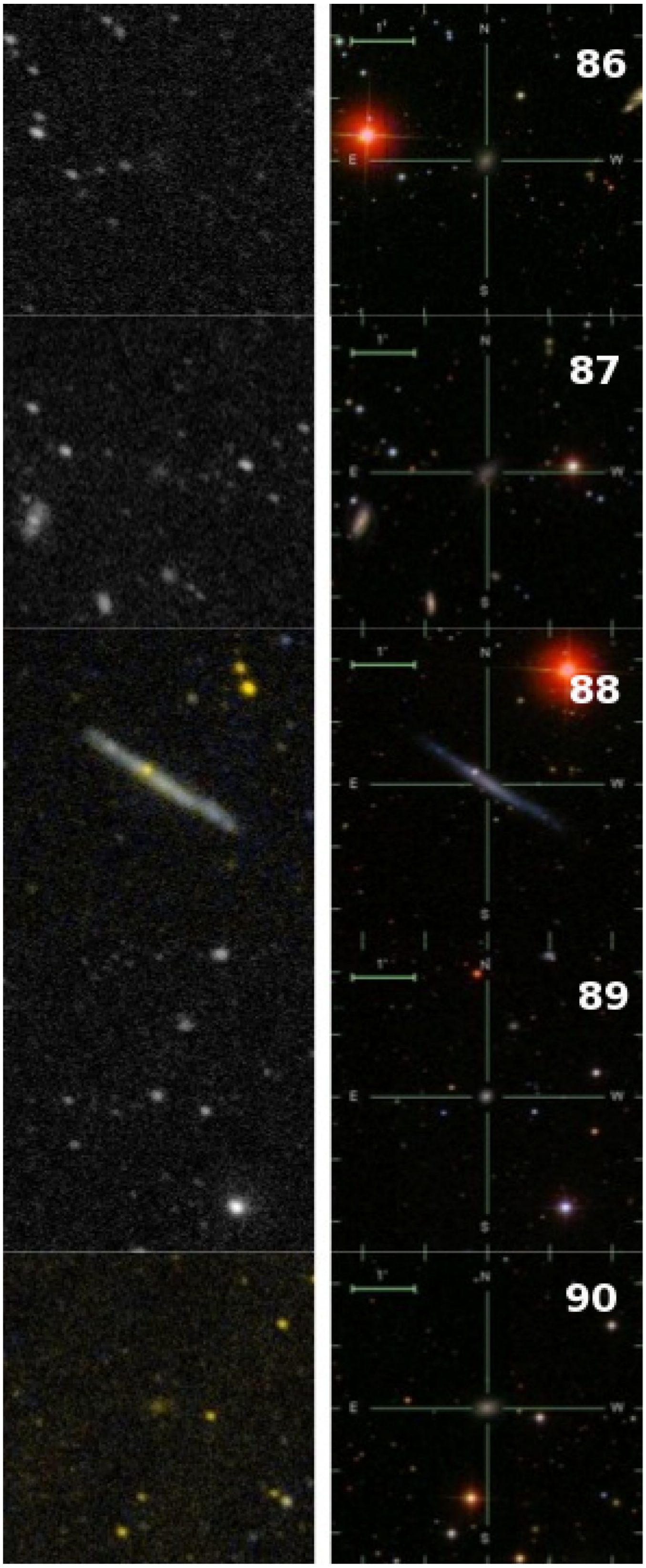

Figure A1 – *continued*

APPENDIX B: THE ENVIRONMENT OF NGC 5846

Table B1. Galaxies in a box of 4 Mpc × 4 Mpc centred on NGC 5846 with heliocentric velocity between 807 and 2600 km s^{-1}.

Galaxies	RA (J2000) (h)	Dec. (J2000) (deg)	Morph. type	Mean Hel. Vel. (km s^{-1})	log D_{25} (arcmin)	log r_{25}	PA (deg)	B_T (mag)
PGC1150067	14.806 85	−0.173 65		2350 ± 60	0.34	0.07	68	18.83 ± 0.33
SDSSJ144834.42+052552.5	14.809 56	5.431 27		1698 ± 1			153.9	18.18 ± 0.5
PGC1241857	14.8397	2.958 19		1697 ± 1	0.56	0.21	166.7	17.18 ± 0.67
SDSSJ145059.85+022016.4	14.849 96	2.3379		1528 ± 24	0.49	0.12	107.3	18.56 ± 0.35
SDSSJ145106.77+023127.0	14.851 89	2.524 15		2071 ± 3	0.49	0.09	79.3	18.53 ± 0.29
SDSSJ145201.94+025841.8	14.867 21	2.978 24		1814 ± 2	0.45	0.02		17.86 ± 0.35
NGC5768	14.868 87	−2.529 76	5.3	1947 ± 8	1.11	0.12	110.9	13.52 ± 0.5
SDSSJ145243.39+043616.7	14.8787	4.604 67		1589 ± 8	0.8	0.49	98.7	17.96 ± 0.5
IC1066	14.884 13	3.296 01	3.2	1567 ± 4	1.08	0.26	69.5	14.27 ± 0.28
IC1067	14.884 79	3.331 75	3	1566 ± 4	1.26	0.09	129	13.62 ± 0.29
NGC5770	14.887 51	3.959 77	−2	1477 ± 15	1.04	0.09		13.18 ± 0.24
NGC5774	14.895 14	3.582 53	6.9	1566 ± 2	1.23	0.21	116.7	13.1 ± 0.51
IC1070	14.897 59	3.484 72	2.4	1677 ± 15	0.89	0.4	121.7	15.94 ± 0.66
NGC5775	14.899 33	3.544 26	5.2	1676 ± 2	1.57	0.64	148.9	12.23 ± 0.13
PGC1223887	14.909 56	2.343 92		2158 ± 42	0.56	0.27	2.4	18.36 ± 0.47
PGC135871	14.911 93	1.161 87	10	1830 ± 7				17.8 ± 0.35
PGC1197564	14.915 51	1.525 56		1759 ± 8	0.49	0.11	70.6	18.77 ± 0.87
PGC1184577	14.919 25	1.100 64		1715 ± 3	0.4	0.18	9.9	18.35 ± 0.28
PGC053365	14.928 58	−1.008 99	9	1849 ± 2	0.8	0.21	43.2	15.78 ± 0.37
UGC09601	14.933 83	−1.387 87	5.9	1862 ± 8	1.09	0.11	171.7	14.62 ± 0.38
PGC1083529	14.938 98	−2.761 59		1888 ± 9	0.41	0.06	85.4	18.66 ± 0.3
PGC184824	14.962 45	−2.987 07	1.6	1800 ± 64	0.61	0.13	130.7	17.14 ± 0.37
PGC184842	14.968 83	−1.312 37	3.8	1947 ± 7	0.75	0.33	149.5	16.45 ± 0.31
NGC5792	14.972 96	−1.090 93	3	1924 ± 2	1.55	0.41	88.5	12.12 ± 0.12
PGC053577	15.000 36	−1.091 07	10	1886 ± 2	0.66	0.03		15.81 ± 0.36
UGC09682	15.075 05	−0.851 35	8.6	1810 ± 4	1.21	0.6	175.2	15.43 ± 0.36
PGC2801020	15.076 16	−2.587	10	1624 ± 2	0.89	0.14	147.8	16.51 ± 0.32
PGC1085904	15.118 93	−2.662 78		2042 ± 1	0.53	0.18	93.2	17.92 ± 0.3
PGC1128787	15.159 33	−1.021 63		1858 ± 1	0.5	0.19	133	17.56 ± 0.35
PGC054159	15.179 78	−0.348 24	6	2159 ± 2	0.91	0.6	86	16.25 ± 0.57
PGC1176138	15.208 81	0.812 56	10	1844 ± 5	0.89	0.31	118.1	16.32 ± 0.29
PGC1200646	15.211 5	1.623 25		1873 ± 4	0.62	0.31	56.3	17.25 ± 0.3
PGC258278	15.2125	6.164 17		1487 ± 8				±
PGC1236445	15.252 62	2.751 83		1764 ± 3	0.78	0.3	56.8	16.89 ± 0.49
PGC054452	15.259 61	2.248 23	−1	1906 ± 2	0.98	0.1	107.5	14.82 ± 0.34
UGC09787	15.2619	1.455 76	9	1589 ± 5	1	0.23	46.9	15.4 ± 0.36
PGC1234821	15.268 32	2.691 96		1463 ± 2	0.72	0.62	169	17.23 ± 0.45
PGC3124577	15.291 51	3.585 48		1883 ± 3	0.58	0.04		17.36 ± 0.35
PGC1168006	15.315 85	0.515 64		2083 ± 14	0.49	0.25	141	18.16 ± 0.33
PGC1230249	15.320 38	2.545 03	4.2	1877 ± 4	0.72	0.18	49.5	16.17 ± 0.35
PGC091432	15.329 97	3.978 06	7.9	1712 ± 8	0.7	0.63	56	±
NGC5913	15.348 73	−2.577 96	1	2002 ± 5	1.27	0.39	173.5	14.02 ± 0.38
NGC5921	15.365 68	5.070 41	4	1430 ± 23	1.48	0.17	140	11.68 ± 0.1
PGC258471	15.377 42	5.829 17		1796 ± 8				±
UGC09830	15.383 56	4.529 17	5.9	1830 ± 5	0.79	0.39	33	15.91 ± 0.62
PGC3123131	15.413 92	3.081 41		1754 ± 1	0.5	0.15	83.5	17.58 ± 0.35

This paper has been typeset from a TEX/LATEX file prepared by the author.